Geoarchaeology

Trachyte of the Euganean Hills (NE Italy): new petrographic and geochemical tracers for recognizing provenance quarry in archaeometry

Journal:	*Geoarchaeology*
Manuscript ID	GEO-17-008
Wiley - Manuscript type:	Research Article
Date Submitted by the Author:	01-Feb-2017
Complete List of Authors:	Germinario, Luigi; Universita degli Studi di Padova, Dipartimento di Geoscienze Hanchar, John; Memorial University of Newfoundland Sassi, Raffaele; Universita degli Studi di Padova, Dipartimento di Geoscienze Maritan, Lara; Universita degli Studi di Padova, Dipartimento di Geoscienze Cossio, Roberto; Universita degli Studi di Torino, Dipartimento di Scienze della Terra Borghi, Alessandro; Universita degli Studi di Torino, Dipartimento di Scienze della Terra Mazzoli, Claudio; Universita degli Studi di Padova, Dipartimento di Geoscienze
Keywords:	Provenance study, Volcanic rock, μ-XRF / SEM-EDS mapping, LA-ICPMS, Multivariate statistical analysis

Trachyte of the Euganean Hills (NE Italy): new petrographic and geochemical tracers for recognizing provenance quarry in archaeometry

Luigi Germinario[1]*, John M. Hanchar[2], Raffaele Sassi[1], Lara Maritan[1], Roberto Cossio[3], Alessandro Borghi[3], Claudio Mazzoli[1]

[1] Department of Geosciences, University of Padova, Via Gradenigo 6, 35131 Padova, Italy
[2] Department of Earth Sciences, Memorial University of Newfoundland, 9 Arctic Avenue, St. John's, NL A1B 3X5, Canada
[3] Department of Earth Sciences, University of Torino, Via Valperga Caluso 35, 10125 Torino, Italy

* Corresponding author: luigi.germinario@gmail.com

ABSTRACT

Trachyte of the Euganean Hills is a subvolcanic porphyritic rock historically used as carving and building stone in northern and central Italy, primarily from the Roman times onwards, with first evidences dating back to Prehistory. The numerous quarries and very similar trachyte varieties, as well as the widespread use of this stone, entail several problems in defining its provenance for archaeological and historical materials. New petrographic and geochemical tracers for recognizing provenance quarry of Euganean trachyte are presented here, providing a comprehensive reference database for archaeometric studies. The petrographic markers principally include quantitative data about mineralogical composition and textural features of phenocrysts and groundmass, determined by image analysis of μ-XRF and SEM-EDS chemical maps, in particular: abundance and grain size distribution of feldspar phenocrysts, phenocrysts-groundmass ratio, content of SiO_2 phases in the groundmass, arrangement and grain size of microlites in the matrix. On the other hand, the geochemical tracers involve composition of bulk rock and phenocrysts, determined by XRF and LA-ICPMS, respectively; quarry recognition can be achieved using plots built from concentrations of major and trace elements, with mineral-scale chemistry being the most effective and precise discriminant parameter, especially referring to biotite and, secondarily, augite, kaersutite and magnetite.

KEYWORDS

Provenance study; Volcanic rock; μ-XRF / SEM-EDS mapping; LA-ICPMS; Multivariate statistical analysis

1. THE EUGANEAN HILLS

The Euganean Hills are a group of hills South-West of the city of Padova (Veneto) in northeastern Italy, covering an area of about 110 km^2 entirely surrounded by the Venetian Plain. Here, the landscape is typically characterized by dome- and cone-shaped reliefs rising up to a maximum elevation of 601 m amsl (M. Venda). These were mainly produced by magmas that intruded into pre-existing sedimentary sequences and creating laccoliths, domes, or dikes; the igneous bodies emplaced at shallow depths were eventually exhumed in a subaerial environment, and their base was later buried by fluvial deposits (Cucato & Mozzi, 2011).

Specifically, the geology of the region is characterized by a deep-water sedimentary succession of limestones and marls dated to the upper Jurassic–lower Oligocene, followed by a Paleogene volcanic and hypabyssal series, and by Quaternary deposits of alluvial origin or derived from weathering of the igneous rocks (Cucato et al., 2011).

The volcanic activity in the Euganean region was part of the Veneto Volcanic Province (VVP). This formed in the upper Paleocene to Oligocene over an area of about 2,000 km^2 between the Garda Lake and Bassano del Grappa-Padova axis, in response to the extensional tectonics of the Southern Alps foreland related to the collision between the Adria and European plates. The Euganean volcanic activity was the latest within the VVP, and included two main events. The first one, upper Eocene in age, was associated with submarine basic and ultrabasic products with alkaline and subalkaline affinity, encompassing pillow and flow lavas, breccias, hyaloclastites and tuffs, known as the Castelnuovo di Teolo formation. The second one, lower Oligocene in age, yielded mostly acid and intermediate subvolcanic rocks, at times combined with effusive and explosive products. Rhyolites and trachytes with moderate Na-alkaline affinity are the most recurring rock types, while latites and basalts subordinately occur, all being included in the M. Venda formation (De Vecchi et al., 1976a; 1976b; De Pieri et al., 1983; Zantedeschi, 1994; Cucato et al., 2011; Bartoli et al., 2015) (Figure 1). This last differentiation was primarily connected to processes of low-pressure fractional

crystallization of mantle-derived basic melts, which took place in multiple shallow magma chambers formed due to block-faulting tectonics, with modest crustal contamination (Milani et al., 1999).

2. QUARRYING ACTIVITY

Euganean trachyte – denomination actually comprising trachytes s.s., quartz-trachytes and less common rhyolites and trachyandesites – is a subvolcanic rock with porphyritic texture and a grey color, often ranging to brown and yellow shades (Figure 2a). It is characterized by excellent durability and technical properties, in particular high resistance to mechanical abrasion and chemical alteration (Calvino, 1969; Zantedeschi & Zanco, 1993; Valluzzi et al., 2005; Graue et al., 2011; Graue, 2013).

Trachyte outcrops have been widely exploited in the course of time, making the Euganean Hills the most important district in Italy for the extraction of this material. Indeed, trachyte also occurs in other Italian regions (Sardinia, Lazio, Tuscany, Campania), in some cases with a notable tradition of use and exploitation (Calvino, 1966; Williams-Thorpe & Thorpe, 1989; De Gennaro et al., 2000; Frulio et al., 2004; Langella et al., 2009), but to a much lesser extent if compared to the commercial relevance of the Euganean district.

Trachyte quarrying in this region is lost to history and started with the first populations settled in the Prehistory, but dramatically increased during the Roman times. The ancient extraction methods involved the use of wedges, inserted into holes in the rock or natural fractures; metallic wedges were hammered inwards, whereas wooden wedges were soaked with water, causing their swelling (Buonopane, 1987; Vergani, 1994). The resulting rock splitting was made easier by columnar, tabular or prismatic jointing that trachyte often displays (Figure 2b). Quarrying methods remained almost unchanged all through the centuries, until introduction of explosives and blasting

technology, experimented already in the 18th century but more frequently from the end of the 19th century onwards. Quarrying continued to be particularly intense at least until the 1960s, then a series of legislative measures (in 1971 and then in 2001) led to a gradual drop in extraction activities, in order to prevent further damage that millennia of excavation caused to the local landscape (Figure 2c). Among the approximately 100 open pits in this area for the extraction of trachyte – 75 of which giving dimension stones (Calvino, 1966) – only four are still active to date (one on M. Merlo and the others on M. Rovarolla).

Most quarries were developed on the edges of hills, which were more easily accessible and closer to residential zones and former settlements. The northwestern hills (M. Altore, M. Comun and M. Rovarolla, near the village Zovon di Vo') have the highest concentration of quarries, but historically the most exploited localities seem to have been those of Monselice, M. Oliveto and M. Merlo, according to the archaeometric literature (Previato et al., 2014).

3. ARCHAEOMETRIC BACKGROUND

3.1. Historical Outline

The diverse use of Euganean trachyte in cultural heritage of northern and central Italy has an age-old tradition (Figure 3), with its first traces dating back to Prehistory (Neolithic, 5th millennium BCE). A higher number of records, however, has been attested from Protohistory and pre-Roman period, within the territories controlled by the Venetic civilization as well as the Etruscans, thanks to mutual trades of raw and finished materials; crafting of querns has been principally reported, but trachyte was also used in buildings, necropolises, for funerary and votive cippi and steles (Cattani et al., 1997, Antonelli et al., 2004; Bianchin Citton & De Vecchi, 2009), even as temper in pottery production (Calogero & Lazzarini, 1984; Maritan, 2004; Maritan et al., 2006).

Subsequently, Roman domination led to a considerable widespread usage of Euganean trachyte (Lazzaro, 1992; Zara, 2016), which was frequently transported by ship along the numerous waterways of the Venetian Plain, the Po river, and in the Adriatic Sea (Renzulli et al., 1999; 2002b); this system was often preferred to small-load transports by animal-drawn carts and sleds. Beside the manufacture of mortars and querns (Cattani et al., 1997; Renzulli et al., 2002a; Antonelli et al., 2004; Antonelli & Lazzarini, 2010; 2012; Santi & Renzulli, 2006), the Romans widely used trachyte for flagstones in paving urban and extra-urban roads – e.g., *Via Flaminia*, *Via Aemilia*, *Via Annia* – as well as for bridges, aqueducts, harbor structures, and milestones (Renzulli et al., 1999; 2002b; Capedri et al., 2000; 2003; Grossi & Zanco, 2003; Santi & Renzulli, 2006; Grossi, 2007; Maritan et al., 2013; Previato et al., 2014). Moreover, the stone was used in private buildings and monuments, especially with structural function, and in funerary contexts, for sarcophagi, tombstones, cippi, urns and steles (Capedri et al., 2003; Capedri & Venturelli, 2003; Previato et al., 2014). According to these findings, the network of trachyte circulation from the Euganean Hills, and therefore from the cities of *Patavium* (Padova) and *Ateste* (Este), extended at distances above 250 km, over a broad, almost quadrilateral area traced by the Roman settlements of *Mediolanum* (Milano)-*Ticinum* (Pavia), Bressanone, *Tergeste* (Trieste)-*Aquileia* and *Ancona-Urbs Salvia* (Urbisaglia) (Figure 3). The Romans often adjusted the selection of the quarries based on their position with respect to transport routes.

Use and trade of Euganean trachyte continued also through the Middle Ages and Renaissance, with the extraction of huge volumes of stone, in addition to the reuse of material from Roman artefacts (Renzulli et al., 1999; Capedri et al., 2000; Capedri & Venturelli, 2005; Marocchi et al., 2009). Especially with the rise of *Serenissima Repubblica di Venezia* (697–1797), stone construction was given a substantial boost, and trachyte was largely employed in public buildings, churches, monasteries, monumental gates, defensive walls, and private residences, as well as for paving squares and streets. The most striking examples can be admired in Venezia and Padova (Negri, 1966; Lazzarini et al., 2008), but stone trades often went as far as the Po Valley and beyond

(Capedri et al., 2000). Diverse applications in urban environments continued in the 19th and 20th century as well (Negri, 1966; Borghi et al., 2015; Lugli et al., 2016).

Today, spread of Euganean trachyte and its use in construction are not limited to northern and central Italy, but also involve central and eastern Europe (e.g., Germany, Austria, Switzerland, Croatia, Netherlands, Russia). Trachyte is mostly used for cladding and paving, but also for restoration of historical architecture, in Italy and abroad, as in the case of excellence of Cologne Cathedral (Graue et al., 2011). Less noble applications comprise street furniture, breakwaters, cladding of structures for industrial treatment of acids and, in the form of aggregate, road foundations and temper in brick production.

3.2. The Provenance Problem

Identifying the provenance quarry of stones used in archaeological or historical objects is a common task in archaeometry. This may involve tracing the ancient trades and circulation routes of raw materials and finished artifacts, reveal historical development of quarrying activities and location of the main sources of stone supply, and guide the choice of proper materials for restoration.

In the case of trachyte of the Euganean Hills, determining the provenance is even more challenging, since this involves a large number of quarries within a single extraction basin, which are very close, in some cases only a few hundred meters apart. This entails the need for carrying out provenance studies at high spatial resolution, in order to cast new light on the following issues: territorial organization of settlements; their areas of political influence; ownership and competition of quarries; localization of extraction and production sites; access to the main trade routes; connection to destination centers and preferred ways of material transport; construction relative chronology within single sites where materials from different quarries were used (e.g., Capedri et al., 2000); use of stone from specific quarries for specific applications.

An additional reason why archaeometry of Euganean trachyte is often essential to historical studies is that written sources about quarrying activities are available only from the 13th century, sporadically though, becoming more frequent and reliable from the end of the 17th century, due to fiscal policy of the *Serenissima* (Vergani, 1994); moreover, the intense exploitation has prevented ancient traces of excavation to be preserved and ancient semi-finished products or artifacts have been found only occasionally on site, for example in the quarries of M. Merlo and M. Oliveto.

From an archaeometric point of view, Euganean trachyte can be easily discriminated from volcanic rocks of other important Italian quarry districts exploited in the antiquity, such as the leucite phonolite and tephritic phonolite of the Vulsini Mounts and Vico volcano in Umbria-Lazio, the basaltic trachyandesite and phonolitic tephrite of Somma-Vesuvius in Campania and the hawaiite and mugearite of the Etna volcano in Sicily. This can be achieved by considering the Na-alkaline affinity of Euganean trachyte and distribution of incompatible trace elements (Santi & Renzulli, 2006), besides petrographic features.

Concerning the differences within the Euganean district itself, a first detailed census of some varieties of Euganean trachyte based on their petrographic and geochemical characteristics was made by Schiavinato (1944). Later on, several datasets reporting bulk-rock chemical compositions (e.g., Calvino, 1969; De Vecchi et al., 1976; De Pieri et al., 1983) and chemistry of phenocrysts (De Pieri et al., 1977; 1978; De Pieri & Molin, 1980; De Pieri & Gregnanin, 1982) were published, although generally referred to few selected sites, until a collection of parameters useful for discriminating Euganean quarries was proposed by Zantedeschi & Zanco (1993). However, the first comprehensive database, which encompasses a higher number of quarry sites and currently represents the reference for archaeometric provenance studies of Euganean trachyte, is that set up by Capedri et al. (2000). Those authors proposed a distinction among the most important trachyte quarries based on textural features, modal composition, bulk chemical composition, and magnetic susceptibility. Despite its accuracy and comprehensiveness, the database has several limitations, discussed later in this paper. Since detailed petrographic characterization turned out to be still

essential, in a recent study Germinario et al. (2016) explored the effectiveness of quantitative petrographic parameters as provenance markers.

In the present paper, new petrographic and geochemical tracers for discriminating and recognizing trachyte quarry localities in the Euganean district are illustrated, building an updated database containing quantitative data about mineralogy, textural features of phenocrysts and groundmass, bulk-rock chemistry and major- and trace-element composition of phenocrysts. The data were treated by means of a robust multivariate statistical approach. The aim is to provide a complete reference support for future provenance studies of Euganean trachyte in archaeometry, by an alternative and more reliable approach than what is currently available in the literature.

4. SAMPLING AND EXPERIMENTAL SETUP

A set of 86 trachyte samples (Table I) were collected covering the entire area of the Euganean Hills, in 40 different outcrops and quarries, most of them inactive and abandoned, localized on 20 different hills (Figure 1). The number of samples from each quarry was chosen depending on its size, presence of other extraction sites in the same quarry locality (i.e., hill) and lithological variability observed in the field. Most of these quarries, where exploitation has been most important or intense, were already sampled by Capedri et al. (2000). All of the analyses aimed at petrographic and geochemical characterization were done on thin sections with a thickness of 45 μm, unless indicated otherwise.

Petrographic investigations were done with a polarized-light optical microscope and a CamScan MX2500 scanning electron microscope (SEM) equipped with a LaB_6 cathode, an EDAX energy-dispersive X-ray spectroscopy (EDS) system and an electron backscattered diffraction (EBSD) detector, at the Department of Geosciences, University of Padova. In addition to standard observations and phase identification, high-resolution X-ray elemental maps were acquired on

selected regions of the rock groundmass, having an area of 0.05 to 1.20 mm^2, depending on the grain size. Operating conditions were 20 kV acceleration voltage and 150 nA beam current and, during map acquisition, a grid of 512 x 400 pixels was scanned using a dwell time of 150 ms per pixel and a time constant of 2.5 µs, applying standard ZAF corrections. The resulting maps were processed by digital image analysis (DIA) through ImageJ and Multispec softwares, as described in Germinario et al. (2016), in order to extract the relative abundances of mineral phases and the following textural features of crystals in the groundmass: area, perimeter, Feret diameter, circularity and aspect ratio.

X-ray elemental maps were also acquired by micro X-ray fluorescence (µ-XRF), but on smoothed stone tiles and large areas of 20 cm^2, using an EDAX Eagle III XPL bench-top spectrometer, at the Department of Earth Sciences, University of Torino. Operating conditions were 40 kV acceleration voltage and 1 mA beam current and, during map acquisition, a grid of 512 x 400 pixels was scanned using a dwell time of 200 ms per pixel, a time constant of 2.5 µs, a spot size of 30 µm and a resolution (step size) of 103.5 µm. The resulting maps were processed by DIA as noted above. Considering the size of the area investigated and the resolution used, mineralogical and textural information was given about phenocrysts and relative abundance of groundmass was calculated, providing the porphyritic index (P.I.). Further details on this method are described in Germinario et al. (2016).

Bulk-rock chemical analyses for major and trace elements were done by X-ray fluorescence (XRF) on glass beads – prepared with calcined samples diluted with $Li_2B_4O_7$ flux in a 1:10 ratio – using a Philips PW2400 spectrometer operating in WD (wavelength dispersive) mode, at the Department of Geosciences, University of Padova. Loss on ignition (LOI) was also determined separately before the XRF analyses.

Finally, the chemical composition of phenocrysts was measured *in situ* on crystals of anorthoclase, plagioclase, sanidine, biotite, augite, kaersutite, Ti-magnetite, and apatite.

The major-element composition was determined by a Cameca Camebax SX 50 electron probe microanalyzer (EPMA), operating in WD mode, using a 15 kV acceleration voltage and a 10 nA beam current, at the Institute for Geosciences and Earth Resources of CNR (CNR-IGG, Padova).

The major- and trace-element composition of the same phenocrysts was also determined by laser ablation inductively-coupled plasma mass spectrometry (LA-ICPMS), using a Thermo Scientific Element XR double-focusing magnetic-sector spectrometer coupled to a GeoLas 193 nm Ar-F excimer laser, at the Micro Analysis Facility of the Bruneau Centre for Research and Innovation, Memorial University of Newfoundland. The laser energy density used for all the analyses was 3 J/cm^2 with a pulse frequency of 8 Hz and a spot size of 40 μm. For each analysis, the background was measured for 30 s, followed by 60 s of laser ablation, and wash out was monitored for 30 s after each ablation, analyzing 2 to 5 spots for each phase on each sample. NIST 610 glass reference material was used as primary calibrant, and analyzed every 10 measurements on the samples; USGS BCR-2G basalt glass reference material and Slyudyanka apatite were also analyzed with the same frequency as secondary standards. Element concentrations were calculated with Iolite v2.5 software package (Paton et al. 2011), based on the NIST 610 signal and the concentrations of selected major elements previously determined by EPMA and used as internal standards[1]: ^{27}Al for anorthoclase, plagioclase, sanidine and biotite, ^{43}Ca for augite, kaersutite and apatite, ^{57}Fe for magnetite.

All the quantitative information obtained with the techniques above was subjected to univariate, bivariate, and multivariate statistical analysis, in particular principal component analysis (PCA) and discriminant analysis, using Statgraphics Centurion XVI software package, in order to identify the most distinctive petrographic and geochemical parameters among the trachyte quarries.

[1] For each mineral phase in each sample, a single EPMA analysis was used as internal standard, considered as mean value for data reduction of the 2 to 5 corresponding spots analyzed by LA-ICPMS. This was considered reliable for the following reasons: exploratory EPMA analyses showed negligible chemical variability of a given mineral phase within the same sample; the crystals analyzed displayed no or very slight zoning under the optical microscope and with cathodoluminescence, or chemical zoning involved elements not used as internal standard; in addition, a set of representative LA-ICPMS analyses was reduced again using as internal standard, for a given phase, the farthest from the average EPMA composition, producing in some cases sensible differences in element concentrations, but maintaining the same relative ratios and basically not affecting sample classification.

5. PETROGRAPHIC TRACERS

5.1. General Characterization

Based on the results of the analyses by optical microscopy, SEM, and EPMA, a general petrographic description will first be provided.

Euganean trachyte is a holocrystalline to hypocrystalline rock with porphyritic texture, often glomeroporphyritic or cumuloporphyritic due to the occurrence of feldspar polycrystalline aggregates, frequently displaying consertal or radiate intergrowths.

The distribution of feldspars consists of anorthoclase, plagioclase, and sanidine, in diverse combinations and proportions. Anorthoclase can be pure end member or calcic, plagioclase has a prevalent oligoclase-andesine composition, while sanidine is mainly pure end member or sodic. Feldspar phenocrysts may be characterized by intracrystalline pores and minute inclusions of glass and feldspar microlites, sometimes zonally arranged, giving a spongy-like appearance; another common feature is overgrowth texture, e.g., plagioclase mantled by an alkali-feldspar corona, or anorthoclase by sanidine. Among mafic minerals, biotite is ubiquitous, often showing Fe-Ti oxide-rich reaction rims and resorbed edges. Clinopyroxene with augite and Fe-augite composition and amphibole with kaersutite composition are sometimes present. In trachytes from several quarries, large crystals of quartz and cristobalite, and occasionally tridymite (verified by SEM-EBSD), also occur. Magnetite, ilmenite, apatite and zircon are the other most recurring accessory minerals, with the first having a Ti-magnetite composition, at times closer to ulvöspinel. Exceptionally, titanite, epidote, calcite, dolomite, monazite and pyrite are present, while siderite – displaying distinctive overgrowths with rhythmic Mg/Ca enrichments – occurs only in the Zovon area (i.e., M. Altore, M. Comun and M. Rovarolla).

Black-greyish xenoliths are common, having a porphyritic, granitoid or weakly schistose texture with usually a trachyandesitic, gabbroic or cornubianitic composition respectively, rich in mafic minerals and magnetite (Sassi et al., 2004; Lazzarini et al., 2008), and are likely derived from the basement rocks through which trachyte intruded. Pervasive oxidation surfaces, constituted by brownish-yellowish migration fronts of Fe oxides and hydroxides, are sometimes visible as well, whereas the content in clay minerals from post-crystallization alteration is generally rather low or negligible.

The groundmass of Euganean trachyte has a microcrystalline to cryptocrystalline grain size, with a composition mainly given by prismatic alkali-feldspar microlites, frequently with fine-grained anhedral SiO_2 minerals (cristobalite and quartz, occasionally tridymite) and glass-bearing domains filling intercrystalline spaces. The texture is usually felty, with microlites being randomly arranged, although preferred orientations are observable also, i.e., trachytic texture, which is hyalopilitic or pilotaxitic depending on whether intercrystalline glass is present or not.

Further details and data useful for provenance determination of Euganean trachyte will be given in the next paragraphs, excluding from the discussion the petrographic outliers detected (in particular the single sample from M. della Madonna).

5.2. Modal Composition

Data about mineralogy and phenocrysts-groundmass ratio obtained by DIA of μ-XRF maps are presented in Table II, while Figure 4 includes some illustrative phase maps obtained after X-ray map processing[2].

A first discriminant parameter among quarries is represented by quantitative ratios of the different feldspar phases in each trachyte variety. PCA performed on the concentrations of anorthoclase,

[2] Only some slight variability in mineral ratios, or absence/presence of minor mineral phases (e.g., plagioclase and augite in Monselice), have been observed in other historical samples of known provenance (unpublished data), so that the data of modal composition of this paper can be considered valid, or at least vey indicative, for ancient quarry faces too.

plagioclase, and sanidine, clearly identifies four main groups (Figure 5a). The first one includes trachytes from the Zovon area, Rocca Pendice and quarry 20 of Monselice, which have high amounts of anorthoclase, from 21 to 29%, and minor quantities of plagioclase (missing in Rocca Pendice and Monselice) and sanidine (missing in Zovon). The second group comprises trachytes from M. Rusta, M. Grande, M. San Daniele, quarry 2 of M. Alto and quarry 21 of Monselice: they all have the highest concentration of sanidine, up to 17%, the lowest concentration on average of plagioclase (totally absent in M. Rusta, M. Grande and Monselice) and often subordinate amounts of anorthoclase. The third group includes only trachytes from M. Bello and M. Lonzina, with the highest quantity of plagioclase, about 20%, the other feldspars being absent or very low. All the other localities are grouped in a fourth large cluster, characterized by negligible amounts of sanidine and an anorthoclase-plagioclase ratio mostly comprised from 1:1 to 3:1.

A second parameter for distinguishing quarries is P.I., which is proportional to the total sum of the feldspar fraction. Trachytes from the Zovon area, quarry 20 of Monselice, Rocca Pendice, M. Bello, M. Lozzo, M. Rosso and M. Merlo are characterized by a P.I. higher than 25%, with groundmass percentage being particularly low (down to about 65%) for the first three localities. On the contrary, the lowest values of P.I., down to 10-15%, are related to M. Cero, M. Murale and M. Trevisan, together with some samples from M. Oliveto and quarry 2 of M. Alto, whereas trachytes from all the other localities are scattered among intermediate values.

Other mineralogical features are less effective as discriminant markers, but some complementary indications can be derived from the concentration of mafic minerals and SiO_2 phases. Total abundance of biotite, augite, and kaersutite is the lowest (under about 1%) in Monselice, M. Rusta, M. Grande, M. San Daniele, M. Oliveto and quarry 2 of M. Alto, and the highest (from 2 to over 3%) in M. Rosso, M. Bello, M. Cero, M. Merlo, M. Lonzina, M. Lozzo and quarry 1 of M. Alto; the simple presence/absence of augite and kaersutite can provide additional clues for discrimination. Concentration of quartz and cristobalite is noticeably high (from 2 to over 5%) only in trachytes from M. Bello, M. San Daniele and single quarries of M. Rusta, M. Oliveto and M. Grande.

5.3. Texture

The most interesting textural feature for quarry clustering derived from the μ-XRF imaging is size of feldspars and feldspar glomeroporphyries, and grain size distribution (Table III, and qualitatively inferable from Figure 4). PCA of the data of feldspar area indicates that trachytes from the Zovon area, Monselice and Rocca Pendice are clearly grouped by their coarse grain size (Figure 5b): the coarsest feldspars exceed 10 mm in diameter, reaching a maximum value of 16 mm, with the highest frequency of crystals above 10 mm^2 in area, and up to 70 mm^2. On the other hand, fine-grained trachytes from M. Murale, M. San Daniele, M. Cero, M. Oliveto and quarry 2 of M. Alto are characterized by nearly all of the feldspar phenocrysts (over 90%) finer than 5 mm^2, often with no crystals in the size classes above 10 mm^2 (Figure 6) and with maximum diameter usually of 5-7 mm. Samples from the other localities range as in Figure 6, mostly in mid grain size classes.

Another discriminant parameter involving grain size distribution can be qualitatively provided through simple optical microscopic observations. Indeed, trachytes from M. Merlo and M. Lozzo have a seriate distribution, and so have those from M. Bello and M. Rosso, together with few samples from M. Oliveto, although to a lesser extent; in contrast, rocks from all the other quarries display an evident hiatal grain size distribution[3] (Figure 7).

5.4. Groundmass

Additional elements for separating and distinguishing the different quarries are composition and texture of the groundmass, studied through SEM-EDS mapping, DIA and optical microscopy

[3] Texture is said to be seriate if crystals of the main mineral phases are distributed within a continuous range of sizes, whereas hiatal texture involves crystals showing few, noticeably different sizes. In this paper, texture with intermediate characteristics is defined as weakly seriate, e.g., in trachytes from M. Bello and M. Rosso: their grain size is distributed in a continuous range only from the fine to the medium size classes (usually up to about 10 mm^2 in area and 5 mm in diameter, according to the μ-XRF results), while one or more hiatuses break the series from the medium to the coarse classes, so that coarse phenocrysts display only few different sizes.

(Table IV). Only a few features turned out to be rather variable within the same sample, i.e., more strictly dependent on the specific mapped portion of the groundmass, such as presence and abundance of glass, iron oxides, other accessory minerals, or microphenocrysts.

On the other hand, the abundance of quartz and cristobalite in the groundmass can be used for identifying a few large quarry clusters. Trachytes from M. Rosso, M. Bello, quarry 2 of M. Alto and quarry 16 of M. Comun are characterized by the highest percentages of the SiO_2 phases, exceeding 20%, while the other quarries of the Zovon area are associated with values from 15 to 20%. At the other extreme are M. Lispida, M. Lozzo, Monselice, M. Cero and M. Murale, which display increasingly lower concentrations, from 10 to nearly 0%. The other localities are scattered over an intermediate or undefined/broad interval.

Another informative mineralogical parameter is the presence and abundance of plagioclase or Ca enriched alkali-feldspars in the rock matrix. Concentration of Ca-rich feldspars ranges from 7 to 13% in quarry 1 of M. Alto, M. Lozzo, M. Murale, M. San Daniele, M. Trevisan and M. Merlo. Slightly lower percentages can be detected for Monselice, M. Rosso and M. Lonzina, whereas for M. Lispida, M. Bello and M. Cero values approach 0%. Ca-rich feldspars are absent in the groundmass of trachytes from all the other localities.

With regard to the groundmass texture, relative arrangement of crystals and grain size can be best analyzed qualitatively under the optical microscope (Figure 7). Since the matrix is almost entirely constituted of alkali-feldspars, the correct separation of single microlites in mutual contact and with the same composition is virtually impossible from X-ray chemical maps.

The groundmass texture is felty in most quarries, while a trachytic texture can be seen in Monselice, M. Cero, M. Murale and M. Trevisan. A mixed felty-trachytic texture can be observed in M. Grande, as well as in few samples from Monselice, M. Oliveto and M. Trevisan, in these last cases being linked to weak isorientation of microlites in domains surrounding the phenocrysts.

As for grain size, a rough distinction among microcrystalline, cryptocrystalline and intermediate matrix is presented in Table IV, where it is worth noting that, on a qualitative basis, the finest-

grained groundmass is that of trachytes from M. Oliveto, M. Lonzina and M. Lispida; conversely, the coarsest grain size is typical of M. Merlo, M. Lozzo, Monselice, and quarry 1 of M. Alto. These considerations are partly validated by quantitative data about grain size of the SiO_2 phases; indeed, mean area of the intercrystalline particles of quartz and cristobalite is proportional to pore-free intercrystalline spaces and, indirectly, to microlite size. This approximation matches in several cases microscopic observations, with the positive correlation between quartz/cristobalite grain size – calculated by SEM-EDS imaging – and related groundmass grain size – observed under the optical microscope.

5.5. Step-by-Step Provenance Recognition

Provenance recognition of Euganean trachyte based on petrography can be accomplished multiple ways, taking into account the parameters described above. Here, a simplified and synthetic procedure, considering one at a time the main petrographic criteria, is suggested and schematically represented in Figure 8. It is possible to start with simple qualitative features easily detectable under the optical microscope, describing grain size distribution and groundmass texture. Image analysis – not necessarily on X-ray maps – is strongly recommended in support of microscopic observations, while going deeper into characterization. In case high uncertainty of provenance attribution of a particular sample arises, the minor petrographic tracers specified in the previous paragraphs will help.

However, contrary to what has been previously stated in the literature, petrographic features alone are not infallible for determining trachyte provenance, especially if a high degree of precision is required, qualitative parameters are mainly considered or a reference collection of quarry samples of known provenance is not available. Indeed, different quarry localities, even far away, can share very similar petrographic features. In addition, within the same quarry or locality, some samples can

display a misleading variability in mineralogical and textural characteristics. This is the case, as an instance, of M. Alto, M. Oliveto and Monselice.

5.6. Comparison with Literature Data

The petrographic markers discussed so far have proven to be the most effective for provenancing purposes. Other criteria suggested in the former literature (Zantedeschi & Zanco, 1993; Capedri et al., 2000) turned out not to have the same reliability.

Rock color is not a useful parameter: besides being rather similar for most trachytes, it can be heavily affected by weathering and Fe oxides/hydroxides migration, the extent of which is independent on the quarry considered.

Determination of modal composition and phenocrysts-groundmass ratio has been previously done by either visual assessment or point counting on thin section, revealing significant inaccuracy especially with regard to correct identification of the different mineral phases and calculation of their quantitative relationships.

Magnetic susceptibility is another parameter suggested as an indirect indicator of mineralogical composition, in particular the abundance of Fe oxides, which however is never uniquely distinctive.

Finally, texture has been previously studied in a qualitative way mostly. Specific features such as feldspar microstructures (e.g., overgrown coronas, internal zoning) and shape are not unequivocally typical of the different quarries, as also confirmed by data of circularity and aspect ratio of phenocrysts acquired by DIA in the present study. Even former determinations of grain size in the literature, performed by naked eye on hand specimens, are less precise and representative than those done by DIA.

The framework of the petrographic analysis proposed here aims at reducing subjectivity and inaccuracy linked to qualitative methods, providing more strict and precise elements for quarry recognition and introducing new criteria.

6. GEOCHEMICAL TRACERS

6.1. General Characterization

According to the total alkali-silica (TAS) classification (Le Maitre, 2002), most samples of Euganean trachyte can be defined as trachyte s.s., based on XRF data of bulk chemical composition. Some of the samples plot in the field of rhyolite, i.e., almost the totality of trachyte samples from M. Rusta and few others from M. Oliveto, M. Alto, M. Grande and M. della Madonna; others more from these localities and M. San Daniele plot very close to the boundary between the two fields (Figure 9). Combining the data of the modal composition determined on phenocrysts and groundmass by μ-XRF and SEM-EDS, and considering the "q" factor (total quartz percentage normalized to the sum of quartz and feldspars), only few samples (from M. Bello, quarry 2 of M. Alto and quarry 36 of M. Rusta) display a value higher than 20%, and then can be classified as trachydacite.

In the following paragraphs, information and plots useful for recognizing provenance quarry of Euganean trachyte will be provided. Few samples (including those previously identified as outliers on petrographic basis, e.g., from M. della Madonna and M. Murale) were recognized as outliers through univariate and multivariate statistical methods applied to their bulk chemical composition, and excluded from the calculations.

6.2. Bulk-Rock Composition

Bulk-rock chemical composition calculated by XRF is reported for all the samples in Supplementary Table 2. These data were used to build binary plots and, among all the possible

combinations, select the pairs of major and trace elements showing the best separations among the Euganean quarry localities; the selection was supported by an explorative PCA done on all the chemical elements analyzed (Supplementary Figure 1), then refined by bivariate statistical analysis. The most informative binary plot is V/Nb, in which the quarry localities of Monselice, M. Rosso, M. Trevisan and M. Merlo (quarry 21 and 23) cluster separately, while the couples M. Bello-M. Lonzina and Zovon area-Rocca Pendice form two mixed clusters (Figure 10); other useful binary plots are TiO_2/Zr, TiO_2/K_2O, Na_2O/Zr, Rb/Zr, Al_2O_3/Sr and Ce/Nd (Figure 11). Few sites can be easily distinguished in multiple binary plots, others cannot be isolated at all, i.e., M. Cero, M. Lispida and quarry 22 of M. Merlo, while the Zovon area and Rocca Pendice cannot be uniquely differentiated from each other. In general, clustering is often not very satisfactory, and attribution of correct provenance may be affected by great uncertainty. This may further increase when analyzing small and altered archaeological objects, instead of fresh quarry samples. For these reasons, in order to minimize possible errors, it is suggested not to rely on single plots and clusters only, but to check the disposition of a study sample using all of the diagrams proposed, and verify which group of reference quarry samples provides the best fit. An alternative could be accomplished by doing a statistical discriminant analysis, using all the data in Supplementary Table 2 in order to classify trachytes from the different quarry localities based on their composition and known provenance, and verifying which locality is attributed by default to the study sample based on multivariate chemical correlations.

6.3. Mineral-Scale Composition

Major-element chemistry of phenocrysts in Euganean trachyte determined by EPMA does not provide useful hints for provenancing after a bivariate and multivariate statistical analysis, since major-element composition of a given phase is rather homogeneous among all the samples, as

indicated by the generally low values of the standard deviations from the mean concentrations in Table V.

The same does not apply to LA-ICPMS results and to major elements when combined with trace elements. All the data obtained from each analyzed spot are included in Supplementary Table 3, subdivided by mineral phase, together with average values measured on 610 and BCR-2G standards.

Initially, the LA-ICPMS data were processed normalizing all the concentrations of rare earth elements (REE) and incompatible elements to CI chondrites and primitive mantle compositions (Sun & McDonough, 1989; McDonough & Sun, 1995). The resulting REE patterns and spider diagrams show negligible variations among the samples and very similar trends for each mineral phase.

The next step was identifying the most informative elements to be used in simple scatterplots for separating quarry localities. A statistical discriminant analysis was performed and all the samples were classified *a priori* according to their known provenance, then the best discriminating multivariate correlations were selected, i.e., linear combinations of major- and trace-element concentrations. These functions were eventually used to build the binary and ternary plots presented below. Traditional binary plots based on concentration values of single elements, similarly to what was done for the XRF data, are also provided in Supplementary Table 4; they can be useful in case of anomalous concentrations obtained for particular elements, which would compromise the efficacy of multivariate correlations.

Biotite is by far the most informative phase, especially considering correlations among Li, Sc, TiO_2, V, MnO and Co, used for the plots in Figure 12, in which a large number of quarry localities cluster separately in a rather well-defined fashion: M. Lispida, M. Lonzina, M. Merlo, M. Rusta, M. San Daniele, M. Trevisan, Monselice and quarry 2 of M. Alto. In addition, the couples Bello-M. Rosso and M. Cero-M. Murale are included in two different mixed clusters; the last two localities can be distinguished in a Co/Zr plot (Supplementary Table 4). The other sites are scattered over broader

intervals of elemental concentration, although their dispersion in the ternary plots is more limited (e.g., for M. Oliveto) and might serve as an indicative guide to try provenance attribution; in this case, however, relying also on other mineral phases is more effective.

When the trachyte to be studied also contains other mafic minerals, one can try to exploit the concentrations of Li, Na_2O, V, Zr in the case of pyroxenes, and Sc, V, Sr, Hf, Th for amphiboles (Figure 13). The relevant discriminant plots are particularly effective, as all the localities in which these mafic minerals were observed on thin section are well separated. Concerning augite, M. Lonzina, M. Lozzo, M. Merlo, M. Rosso, Zovon, quarry 31 of M. Oliveto and quarry 32 of Rocca Pendice. Concerning kaersutite, M. Lozzo, M. Merlo, M. Oliveto, M. Trevisan, Monselice and quarry 1 of M. Alto. Complementary traditional binary plots are reported in Supplementary Table 4.

Among the accessory minerals, apatite composition does not show any systematic variation related to provenance quarry, whereas magnetite chemistry represents a valid support for aiding quarry attribution when the results obtained on mafic minerals are still questionable. As shown in Figure 13, several quarry sites cluster separately in a plot based on linear combinations of MgO, V, MnO and Co concentrations, although with some ambiguous groups and overlapping. Nevertheless, the advantage of considering magnetite is that – contrary to augite or kaersutite – it is ubiquitous in Euganean trachyte, and provides better separations for M. Bello, M. Oliveto, M. Rosso and Zovon. Again, additional supporting plots can be consulted in Supplementary Table 4.

Finally, and somewhat surprisingly, feldspars turned out to be source of only a limited amount of information for provenancing, and discriminant analysis was more complex, requiring and involving a larger number of elements to produce some sort of quarry clustering (Figure 14). Indeed, analysis of feldspars should be generally unnecessary, or considered only in a final step, for further confirming previous findings or when provenance achieved with the other phases is still undetermined. Considering anorthoclase, combinations of Li, Sc, TiO_2, Sr, La, Eu and Pb allow separating the quarry localities of M. Grande, M. Rosso, M. San Daniele, M. Trevisan, Rocca Pendice and Zovon, but with a partial overlapping. For sanidine, combinations of Li, TiO_2, Rb, Sr,

Ce, Eu and Pb lead to distinguish quarry groups for M. Grande, M. Lozzo, M. San Daniele, Rocca Pendice and quarry 2 of M. Alto, while M. Bello and M. Rosso plot in the same field. Finally, plagioclase results to be suitable only for recognizing the localities of Zovon, M. Trevisan and quarry 2 of M. Alto, applying the concentrations of Li, Sc, TiO_2, Sr, La and Eu. For all the feldspars, as for all the other mineral phases, additional binary plots, built with pairs of the chemical elements mentioned before, are provided in Supplementary Table 4.

Globally, quarry clustering achieved at the mineral scale with LA-ICPMS data is definitely more precise and effective than that obtained on bulk rock with XRF, and this applies to nearly all the Euganean quarry localities, especially if analyses of different phases are cross-matched. As already suggested previously, however, it is advisable to plot concentrations on multiple discriminant diagrams, even when only a single phase is analyzed.

6.4. Comparison with Literature Data

As the LA-ICPMS data are introduced here for the first time referring to Euganean trachyte, the only possible comparison with previously published geochemical data involves the XRF results of this paper and those from the database by Capedri et al. (2000), the most complete collection of bulk-compositional data of Euganean trachyte so far.

Maritan et al. (2013) already outlined a discrepancy between the concentrations of some elements (e.g., Ti, Th, Sr, Zr) reported in the reference database and those published later, determined by either XRF or ICP-MS, even by the same authors of the database (Renzulli et al., 2002b; Capedri et al., 2003; Capedri & Venturelli, 2003; 2005; Antonelli et al., 2004; Antonelli & Lazzarini, 2012). This is further confirmed here and illustrated in Figure 15 in the Sr/Th plot, the main discriminant diagram by Capedri et al. (2000), in which the mismatch between the samples of the reference database and those studied in this paper is evident. The same applies to the other reference binary plots. This seems to confirm the hypothesis of Maritan et al. (2013) that powder grain size in the

pellets prepared by Capedri et al. (2000) was not fine enough to prevent matrix, microabsorption and enhancement effects, leading to low data accuracy of the XRF analyses.

Therefore, besides the fact that discrimination of Euganean trachyte based exclusively on bulk composition is not fully reliable, it is recommended to use the new discriminant binary plots here proposed, when only XRF data are available.

7. CONCLUSIONS

A new reference database of petrographic and geochemical data for trachyte of the Euganean Hills, based on samples from 40 different quarries, has been established in support of archaeometric studies aimed at understanding stone provenance in artifacts and structures of archaeological and historical significance. Proposing an alternative and more reliable approach than that presently available from the literature, this paper describes several provenance markers referred to mineralogy, texture, bulk-rock and mineral-scale chemistry of Euganean trachyte, providing mainly quantitative data and objective criteria for quarry recognition.

This study discriminates among hills and quarry localities, but not among single quarries within the same locality. In fact, trachytes from different quarries but belonging to the same geological body are obviously extremely hard to distinguish. Moreover, such a high-resolution investigation, in this case, would be of scarce significance for archaeometric purposes.

Standard petrographic observations of thin sections, and analysis of bulk chemical composition, the most traditional methodologies previously used, might both be applied to solve provenance problems of Euganean trachyte. However, in most cases, differences of petrographic features and bulk composition among different quarry sites are subtle, and provenancing may be accurate only combining the two techniques, although still not univocal. The use of quantitative petrographic parameters from image analysis of X-ray elemental maps – or even optical images – considerably

improves attribution reliability. On the other hand, success of a study based on XRF (or bulk ICP-MS) can be compromised by insufficient compositional representativeness of samples, a major drawback when dealing with archaeological materials, the sampling of which may be restricted to very small portions, in some cases also having altered surfaces.

Alternatively, *in situ* LA-ICPMS analysis at the mineral scale has proven to be a precise, accurate, and highly sensitive method for autonomously recognizing virtually all the Euganean quarry localities, using major- and trace-element composition of phenocrysts. Besides higher reliability of provenance attribution, the amount of material required for the analyses is very limited: at best, even few fine-grained crystals – for representativeness reasons – of a single diagnostic phase might be sufficient, and this is a great advantage in the study of cultural heritage, when non-destructive or micro-destructive techniques are mandatory. Moreover, although LA-ICPMS may work as a stand-alone technique, one could choose to couple a petrographic examination, in this case a single thin section of suitable thickness (40-50 μm) would be needed (to avoid drilling through the sample during the LA-ICPMS analyses).

In summary, although a standard petrographic study is fast and cost-effective, interpretation is complex and may lead to some degree of uncertainty in quarry identification. On the other hand, mineral-scale chemical analysis of major and trace elements is undoubtedly more expensive and requires greater effort in data processing, but provides univocal results and can be applied to considerably smaller samples.

The improved precision of the novel methodology proposed here might call into question some of the provenance determinations made in the past, which might have introduced a misleading bias in the following provenance studies, with possible consequences on the global archaeometric record of Euganean trachyte.

ACKNOWLEDGEMENTS

The authors thank Anne Westhues (MUN, St. John's), Raul Carampin (CNR-IGG, Padova), Richard Spiess and Leonardo Tauro (Uni. Padova) for their support during the LA-ICPMS, EPMA and SEM analyses, respectively. The authors are very grateful to Arturo Zara and Jacopo Bonetto (Uni. Padova) for the constant exchange of information and ideas concerning the archaeological background. The reviews and comments on an early draft of the manuscript by Giuseppe Cultrone (Uni. Granada) and Siegfried Siegesmund (Uni. Göttingen) are also much appreciated. Thanks are due to the owners of the quarries of Zovon (Martini Costruzioni s.r.l., Toniolo s.r.l., Trachite Euganea s.r.l.) and Montemerlo (Cave Pietra Montemerlo s.r.l.) and, in particular, to Michelangelo Dalla Francesca, for providing trachyte samples and information about quarry activities. Musei Civici di Padova and, in particular, Francesca Veronese are also thanked for photographic material and information about trachyte artifacts in Padova. Finally, the authors are grateful to Silvio Capedri, Riccardo Grandi (Uni. Modena-Reggio Emilia) and Gianpiero Venturelli (Uni. Parma) for their previous inspiring work on the same topic.
This research was supported by the University of Padova (Research Project No. CPDA151883/15) and NSERC (Natural Sciences and Engineering Research Council, Canada Discovery Grant to JMH).

REFERENCES

Antonelli, F., Bernardini, F., Capedri, S., Lazzarini, L., & Montagnari Kokelj, E. (2004). Archaeometric study of protohistoric grinding tools of volcanic rocks found in the Karst (Italy-Slovenia) and Istria (Croatia). *Archaeometry*, 46 (4), 537–552.

Antonelli, F., & Lazzarini, L. (2010). Mediterranean trade of the most widespread Roman volcanic millstones from Italy and petrochemical markers of their raw materials. *Journal of Archaeological Science*, 37, 2081–2092.

Antonelli, F., & Lazzarini, L. (2012). The first archaeometric characterization of Roman millstones found in the Aquileia archaeological site (Udine, Italy). *Archaeometry*, 54 (1), 1–17.

Bartoli, O., Meli, S., Bergomi, M.A., Sassi, R., Magaraci, D., & Liu, D.Y. (2015). Geochemistry and zircon U-Pb geochronology of magmatic enclaves in trachytes from the Euganean Hills (NE Italy): further constraints on Oligocene magmatism in the eastern Southern Alps. *European Journal of Mineralogy*, 27, 161–174.

Bianchin Citton, E., & De Vecchi, G. (2009). L'impiego della trachite euganea nella fabbricazione di macine in età preromana. In E. Bianchin Citton E., S. Rossi, & P. Zanovello (Eds.), *Dinamiche insediative nel territorio dei Colli Euganei dal Paleolitico al Medioevo. Atti del convegno di studi* (pp. 139–150), Este & Monselice, Italy, 27–28 November 2009.

Borghi, A., Berra, V., D'Atri, A., Dino, G.A., Gallo, L.M., Giacobino, E., Martire, L., Massaro, G., Vaggelli, G., Bertok, C., Castelli, D., Costa, E., Ferrando, S., Groppo, C., & Rolfo, F. (2015). Stone materials used for monumental buildings in the historical centre of Turin (NW Italy): architectonical survey and petrographic characterization of Via Roma. In D. Pereira et al. (Eds.), *Global heritage stone: towards international recognition of building and ornamental stones* (pp. 201–218), Special Publications, 407. London: Geological Society.

Buonopane, A. (1987). Estrazione, lavorazione e commercio dei materiali lapidei. In E. Buchi (Ed.), *Il Veneto nell'età romana* (pp. 186–218). s.l.: Banca Popolare di Verona.

Buxeda i Garrigós, J. (1999). Alteration and contamination of archaeological ceramics: the perturbation problem. *Journal of Archaeological Science*, 26, 295–313.

Buxeda i Garrigós, J., & Kilikoglou, V. (2003). Total variation as a measure of variability in chemical data sets. In L. van Zelst (Ed.), *Patterns and process* (pp. 185–198). Suitland, MD: Smithsonian Center for Materials Research and Education.

Calogero, S., & Lazzarini, L. (1984). Caratterizzazione chimico-fisica di ceramiche grigie dallo scavo dell'area ex Pilsen a Padova. *Archeologia Veneta*, 7, 81–97.

Calvino, F. (1966). *Le cave dei Colli Euganei*. Padova: Consorzio per la valorizzazione dei Colli Euganei.

Calvino, F. (1969). Studi sulle proprietà tecniche della trachite da taglio di Montemerlo (Colli Euganei). *Memorie degli Istituti di Geologia e Mineralogia dell'Università di Padova*, 27, 3–39.

Capedri, S., Grandi, R., & Venturelli, G. (2003). Trachytes used for paving Roman roads in the Po Plain: characterization by petrographic and chemical parameters and provenance of flagstones. *Journal of Archaeological Science*, 30, 491–509.

Capedri, S., & Venturelli, G. (2003). Trachytes employed for funerary artefacts in the Roman Colonies Regium Lepidi (Reggio Emilia) and Mutina (Modena) (Italy): provenance inferred by petrographic and chemical parameters and by magnetic susceptibility. *Journal of Cultural Heritage*, 4, 319–328.

Capedri, S., & Venturelli, G. (2005). Provenance determination of trachytic lavas, employed as blocks in the Romanesque cathedral of Modena (Northern Italy), using magnetic susceptibility, and petrographic and chemical parameters. *Journal of Cultural Heritage*, 6, 7–19.

Capedri, S., Venturelli, G., & Grandi, R. (2000). Euganean trachytes: discrimination of quarried sites by petrographic and chemical parameters and by magnetic susceptibility and its bearing on the provenance of stones of ancient artefacts. *Journal of Cultural Heritage*, 1, 341–364.

Cattani, M., Lazzarini, L., & Falcone, R. (1997). Macine protostoriche dall'Emilia e dal Veneto: note archeologiche, caratterizzazione chimico-petrografica e determinazione della provenienza. *Padusa*, 31, 105–137.

Cucato, M., De Vecchi, G., & Sedea, R. (2011). Inquadramento geologico. In M. Cucato et al. (Eds.), *Note illustrative della Carta Geologica d'Italia alla scala 1:50.000, Foglio 147, Padova sud* (pp. 27–31). Padova: ISPRA.

Cucato, M., & Mozzi, P. (2011). Inquadramento geomorfologico. In M. Cucato et al. (Eds.), *Note illustrative della Carta Geologica d'Italia alla scala 1:50.000, Foglio 147, Padova sud* (pp. 17–25). Padova: ISPRA.

De Gennaro, M., Calcaterra, D., Cappelletti, P., Langella, A., & Morra, V. (2000). Building stone and related weathering in the architecture of the ancient city of Naples. *Journal of Cultural Heritage*, 1, 399–414.

De Pieri, R., De Vecchi, G., Gregnanin, A., & Piccirillo, E.M. (1977). Trachyte and rhyolite feldspars in the Euganean Hills (Northern Italy). *Memorie di Scienze Geologiche*, 32, 1–22.

De Pieri, R., & Gregnanin, A. (1982). Trachyte amphiboles in the Euganean Hills (North-eastern Italy). *Rendiconti della Società Italiana di Mineralogia e Petrologia*, 38 (2), 657–666.

De Pieri, R., Gregnanin, A., & Piccirillo, E.M. (1978). Trachyte and rhyolite biotites in the Euganean Hills (North-eastern Italy). *Neues Jahrbuch für Mineralogie Abhandlungen*, 132 (3), 309–328.

De Pieri, R., Gregnanin, A., & Sedea, R. (1983). Guida alla escursione sui Colli Euganei. *Memorie della Società Geologica Italiana*, 26, 371–381.

De Pieri, R., & Molin, G.M. (1980). Trachyte pyroxenes in the Euganean Hills (North-eastern Italy). *Neues Jahrbuch für Mineralogie Abhandlungen*, 138 (1), 64–80.

De Vecchi, G., Gregnanin, A., & Piccirillo, E.M. (1976a). Aspetti petrogenetici del vulcanesimo terziario veneto. *Memorie degli Istituti di Geologia e Mineralogia dell'Università di Padova*, 30, 1–32.

De Vecchi, G., Gregnanin, A., & Piccirillo, E.M. (1976b). Tertiary volcanism in the Veneto: magmatology, petrogenesis and geodynamic implications. *Geologische Rundschau*, 65 (1), 701–710.

Frulio, G., Langiu, M.R., & Mameli P. (2004). L'impiego della trachite nelle architetture tra gli anni Venti e Cinquanta in Sardegna: tecniche costruttive e materiali tradizionali tra nuove tecnologie e modernità. In G. Biscontin, & G. Driussi (Eds.), *Architettura e materiali del Novecento: conservazione, restauro, manutenzione. Atti del convegno di studi* (pp. 465–476), Bressanone, Italy, 13–16 July 2004.

Germinario, L., Cossio, R., Maritan, L., Borghi, A., & Mazzoli, C. (2016). Textural and mineralogical analysis of volcanic rocks by μ-XRF mapping. *Microscopy and Microanalysis*, 22, 690–697.

Graue, B. (2013). Stone deterioration and replacement of natural building stones at the Cologne cathedral. A contribution to the preservation of cultural heritage. Unpublished doctoral dissertation, Georg-August-Universität Göttingen.

Graue, B., Siegesmund, S., & Middendorf, B. (2011). Quality assessment of replacement stones for the Cologne Cathedral: mineralogical and petrophysical requirements. *Environmental Earth Sciences*, 63, 1799–1822.

Grossi, P., & Zanco, A. (2003). Miliari romani nel Nord Italia: materiali, provenienza, lavorazione. L'esempio dell'area Veneta e Friulana. *Quaderni di archeologia del Veneto*, 19, 192–202.

Grossi, P. (2007). Pietre miliari della VIII Regio: analisi litologiche, provenienza dei materiali e loro distribuzione. *Epigraphica*, 69, 181–207.

Langella, A., Calcaterra, D., Cappelletti, P., Colella, A., D'Albora, M.P., Morra, V., & De Gennaro, M. (2009). Lava stones from Neapolitan volcanic districts in the architecture of Campania region, Italy. *Environmental Earth Sciences*, 59, 145–160.

Lazzarini, L., Antonelli, F., Cancelliere, S., Conventi, A. (2008). The deterioration of Euganean trachyte in Venice. In J.W. Lukaszewicz, & P. Niemcewicz (Eds.), *Proceedings of the 11th International Congress on Deterioration and Conservation of Stone* (pp. 153–163), Torun, Poland, 15–20 September 2008.

Lazzaro, L. (1992). Cave di trachite ed uso della pietra trachitica in età romana. *Padova e il suo territorio*, 37, 38–40.

Le Maitre, R.W., Ed. (2002). *Igneous rocks: a classification and glossary of terms* (2nd ed.). Cambridge: Cambridge University Press.

Lugli, S., Caroselli, M., Marchetti Dori, S., Vandelli, V., Marzani, G., Segattini, R., Bianchi, C., & Weber, J. (2016). Building materials and degradation phenomena of the Finale Emilia Town Hall (Modena): an archaeometric study for the restoration project after the 2012 earthquake. *Periodico di Mineralogia*, 85, 59–67.

Maioli, M.G., & Stoppioni, M.L. (1987). *Classe e Ravenna fra terra e mare*. Ravenna: Sirri.

Maritan, L. (2004). Archaeometric study of Etruscan-Padan type pottery from the Veneto region: petrographic, mineralogical and geochemical-physical characterisation. *European Journal of Mineralogy*, 16, 297–307.

Maritan, L., Mazzoli, C., Rigaldo, P., Pesavento Mattioli, S., & Mazzocchin, S. (2006). Le olle romane dello scavo di via Neroniana (Montegrotto Terme – Padova): indagini preliminari. In C. D'Amico (Ed.) *Atti del Convegno AIAr* (pp. 253–260), Caserta, Italy, 16–18 February 2005.

Maritan, L., Mazzoli, C., Sassi, R., Speranza, F., Zanco, A., & Zanovello, P. (2013). Trachyte from the Roman aqueducts of Padua and Este (north-east Italy): a provenance study based on petrography, chemistry and magnetic susceptibility. *European Journal of Mineralogy*, 25, 415–427.

Marocchi, M., Dellisanti, F., Bargossi, G.M., Gasparotto, G., Grillini, G.C., & Rossi, P.L. (2009). Mineralogical-petrographic characterisation and provenance of "Porta Nuova" stones: a XVI century gate in Ravenna (Italy). *Periodico di Mineralogia*, 78, 13–28.

McDonough, W.F., & Sun, S.-s. (1995). The composition of the Earth. *Chemical Geology*, 120, 223–253.

Milani, L., Beccaluva, L., & Coltorti, M. (1999). Petrogenesis and evolution of the Euganean Magmatic Complex, Veneto Region, North-East Italy. *European Journal of Mineralogy*, 11, 379–399.

Negri, A. (1966). L'impiego della trachite euganea nei monumenti storici in Padova. *Marmo Tecnica Architettura*, 7, 89–100.

Paton, C., Hellstrom, J., Paul, B., Woodhead, J., & Hergt, J. (2011). Iolite: Freeware for the visualisation and processing of mass spectrometric data. *Journal of Analytical Atomic Spectrometry*, 26, 2508–2518.

Piccoli, G., Sedea, R., Bellati, R., Di Lallo, E., Medizza, F., Girardi, A., De Pieri, R., De Vecchi, G., Gregnanin, A., Piccirillo, E.M., Norinelli, A., & Dal Prà, A. (1981). Note illustrative della Carta geologica dei Colli Euganei alla scala 1:25000 – II edizione. *Memore di Scienze Geologiche*, 34, 523–566.

Previato, C., Bonetto, J., Mazzoli, C., & Maritan, L. (2014). Aquileia e le cave delle regioni alto-adriatiche: il caso della trachite euganea. In J. Bonetto, S. Camporeale, & A. Pizzo (Eds.), *Arqueología de la construcción IV. Las canteras en el mundo antiguo: sistemas de explotación y procesos productivos* (pp. 149–166). Mérida: CSIC.

Renzulli, A., Antonelli, F., Santi, P., Busdraghi, P., & Luni, M. (1999). Provenance determination of lava flagstones from the Roman 'Via Consolare Flaminia' pavement (central Italy) using petrological investigations. *Archaeometry*, 41 (2), 209–226.

Renzulli, A., Santi, P., Nappi, G., Luni, M., & Vitali, D. (2002a). Provenance and trade of volcanic rock millstones from Etruscan-Celtic and Roman archaeological sites in Central Italy. *European Journal of Mineralogy*, 14, 175–183.

Renzulli, A., Santi, P., Serri, G., & Luni, M. (2002b). The Euganean trachyte flagstones ("basoli") used by the Romans along the mid-Adriatic coast (Marche, central Italy): an archaeometric study. *Periodico di Mineralogia*, 71, 189–201.

Santi, P., & Renzulli, A. (2006). Italian volcanoes as landmarks for the spreading of trade networks during the Etruscan and Roman periods: the millstones and flagstones case study. *Acta Vulcanologica*, 18 (1-2), 133–140.

Sassi, R., Mazzoli, C., Spiess, R., & Cester, T. (2004). Towards a better understanding of the fibrolite problem: the effect of reaction overstepping and surface energy anisotropy. *Journal of Petrology*, 45 (7), 1467–1479.

Schiavinato, G. (1944). Studio chimico-petrografico dei Colli Euganei. *Memorie dell'Istituto Geologico dell'Università di Padova*, 15, 1–59.

Selmin, F., Ed. (2005). *I Colli Euganei*. Sommacampagna: Cierre.

Sun, S.-s., & McDonough, W.F. (1989). Chemical and isotopic systematics of oceanic basalts: implications for mantle composition and processes. In A.D. Saunders, & M.J. Norry (Eds.), *Magmatism in the Ocean Basins* (pp. 313–345), Special Publication, 42. Oxford: Geological Society.

Valluzzi, M.R., Mazzoli, C., Maritan, L., Bianchini, G., & Andreoli, F. (2005). Experimental analyses for the preservation of trachyte pavings in salt-controlled weathering conditions. In N. Banthia, T. Uomoto, A. Bentur, & S.P. Shah (Eds.), *Construction materials: proceedings of ConMat '05 and Mindness Symposium* (pp. 1–10), Vancouver, Canada, 22–24 August 2005.

Vergani, R. (1994). Masegne e calchere: secoli di attività estrattiva. In A. Rigon (Ed.), *Monselice. Storia, cultura e arte di un centro "minore" del Veneto* (pp. 403–413). Monselice: Canova.

Whitney, D.L., & Evans, B.W. (2010). Abbreviations for names of rock-forming minerals. *American Mineralogist*, 95, 185–187.

Williams-Thorpe, O., & Thorpe, R.S. (1989). Provenancing and archaeology of Roman millstones from Sardinia (Italy). *Oxford Journal of Archaeology*, 8 (1), 89–117.

Zantedeschi, C. (1994). New Rb-Sr radiometric data from Colli Euganei (North-Eastern Italy). *Memorie di Scienze Geologiche*, 46, 17–22.

Zantedeschi, C., & Zanco, A. (1993). Distinctive characteristics of euganean trachytes for their identification in ancient monuments. *Science and Technology for Cultural Heritage*, 2, 1–10.

Zara, A. (2016). La trachite euganea: approvvigionamento, impiego e diffusione in età romana. Unpublished doctoral dissertation, Università degli Studi di Padova.

FIGURE CAPTIONS

Figure 1. Geological map of the Euganean Hills (modified after Piccoli et al., 1981). The named hills represent the sampled quarry localities, and each of the 40 sampled quarries is marked and localized with a reference progressive number (coordinates of each sampling point in Supplementary Table 1). "M." in the proper name of the hills stands for "Monte" (mount). The peak of the highest hill, M. Venda (601 m a.m.s.l.), is indicated with a black triangle.

Figure 2. a) Macroscopic appearance of Euganean trachyte (sample from M. Rovarolla); **b)** quarry face of M. Merlo in 2009, displaying columnar and prismatic jointing (courtesy of Michelangelo Dalla Francesca); **c)** quarry of Monselice in late 19th-early 20th century (Selmin, 2005): part of the Medieval architectonic complex on the hill has been lost due to excavation activity.

Figure 3. Historical use of Euganean trachyte: **a)** indication of the area of trachyte circulation in the Roman times (shaded) and principal extra-urban roads; **b)** Roman road with trachyte flagstones in Classe, the ancient port of Ravenna, 4–6th c. CE (Maioli & Stoppioni, 1987); **c)** funerary stele of Oppi family, Padova, 1st c. CE (courtesy of Musei Civici di Padova, Gabinetto Fotografico); **d)** Roman rotary querns, Padova (courtesy of Musei Civici di Padova, Gabinetto Fotografico); **e)** arcade of Palazzo della Ragione, Padova, 13–14th c. CE; **f)** Basilica of Sant'Antonio of Padova, 13–14th c. CE, with trachyte pillars and buttresses, and on the left the equestrian statue of Gattamelata by Donatello, 15th c. CE, with trachyte base; **g)** Basilica of San Marco, Venezia, 11th–17th c. CE, in Piazza San Marco, 12th–19th c. CE, paved with trachyte; **h)** Cologne Cathedral, 13–19th c. CE, with replacing ashlars in Euganean trachyte.

Figure 4. Phase maps of Euganean trachyte processed from X-ray maps acquired by µ-XRF, on a surface of 5.30x4.14 cm of samples from: **a)** M. Altore, quarry 14, characterized by high concentration of anorthoclase, high P.I. and coarse grain size; **b)** M. San Daniele, quarry 39, with high amount of sanidine and fine grain size; **c)** M. Bello, quarry 3, displaying high content of plagioclase and medium-high P.I.; **d)** M. Cero, quarry 5, with an anorthoclase-plagioclase ratio of ~1:1, low P.I. and fine grain size. Mineral abbreviations as in Table II, colors not in the legend indicate minor phases.

Figure 5. Results of PCA performed on µ-XRF data of trachyte quarries, with score and loading plots built on the following parameters: **a)** average concentration of feldspars (anorthoclase, plagioclase and sanidine), with PC1 and PC2 covering 49% and 41% of total variance, respectively; **b)** frequency size classes of feldspars expressed as area, with PC1 and PC2 covering 83% and 10% of total variance, respectively. Quarry symbols as in Table I.

Figure 6. Frequency histogram of size classes of feldspars expressed as area, determined by DIA of µ-XRF maps for each trachyte quarry. Quarries are indicated with locality name and ID number in parentheses.

Figure 7. Thin-section photomicrographs of Euganean trachyte, with samples from: **a)** M. Merlo, quarry 22, showing a seriate grain size distribution (plane-polarized light); **b)** M. Rosso, quarry 34, displaying a weakly seriate grain size distribution (plane-polarized light); **c)** M. Oliveto, quarry 31, with a hiatal distribution (plane-polarized light); **d)** Monselice, quarry 20, having a microcrystalline groundmass with trachytic texture (crossed-polarized light); **e)** M. Rovarolla, quarry 12, with a microcrystalline felty groundmass (crossed-polarized light); **f)** M. Oliveto, quarry 30, characterized by a cryptocrystalline groundmass (crossed-polarized light). Anomalous colors are due to the 45 µm thickness of the sections.

Figure 8. Practical flowchart-like scheme for recognizing quarry locality of provenance of Euganean trachyte, starting from one of the three kinds of grain size distribution. Only few, significant petrographic parameters are considered here, so that it is necessary to refer to the text and tables (Table II, III, IV) for precise attribution, quantitative data and to try discriminating analogous sites. Feldspars abbreviations according to Whitney & Evans (2010).

Figure 9. Disposition of the samples of Euganean trachyte in the TAS (total alkali-silica) classification diagram (Le Maitre, 2002), based on bulk-rock chemical composition determined by XRF.

Figure 10. V vs. Nb scatterplot from bulk-rock chemical composition determined by XRF for all the samples of Euganean trachyte. Quarry symbols as in Table I.

Figure 11. Binary scatterplots from bulk-rock chemical composition determined by XRF for all the samples of Euganean trachyte. Quarry symbols as in Table I.

Figure 12. Plots from chemical composition of biotite in Euganean trachyte determined by LA-ICPMS, with major elements expressed as oxide weight percent and trace elements as ppm, using the isotopes in Supplementary Table 3: **top)** scatterplots after statistical discriminant analysis, with variables calculated from multivariate combinations of element concentrations, indicated under each relevant graph; **bottom)** ternary plots, scaled up as indicated in the miniature. Quarry symbols as in Table I.

Figure 13. Scatterplots from chemical composition of augite, kaersutite and Ti-magnetite in Euganean trachyte determined by LA-ICPMS, with major elements expressed as oxide weight percent and trace elements as ppm, using the

isotopes in Supplementary Table 3; variables are calculated from multivariate combinations of element concentrations, indicated under each relevant graph, after statistical discriminant analysis. Quarry symbols as in Table I.

Figure 14. Scatterplots from chemical composition of feldspars in Euganean trachyte determined by LA-ICPMS, with trace elements expressed as ppm, using the isotopes in Supplementary Table 3; variables are calculated from multivariate combinations of element concentrations, indicated under each relevant graph, after statistical discriminant analysis. Quarry symbols as in Table I.

Figure 15. Sr vs. Th scatterplot from bulk-rock chemical composition determined by XRF on Euganean trachyte – the main discriminant diagram by Capedri et al. (2000) – showing the mismatch among the samples from this work (large indicators) and the corresponding ones from the reference database (small indicators). Quarry symbols as in Table I.

SUPPLEMENTARY MATERIAL CAPTIONS

Supplementary Figure 1. Score and loading plot from PCA performed on bulk-rock chemical composition of Euganean trachyte determined by XRF for all the samples, with PC1 and PC2 covering 37% and 16% of total variance, respectively (quarry number and localization as in Figure 1, symbols as in Table I). All the measured elements were considered, since none of them showed anomalous concentrations, which might be detected after weathering, or crystallization of secondary phases; this was verified examining the compositional variation matrix and variance of each element, namely the "τ.i" value (Buxeda i Garrigós, 1999; Buxeda i Garrigós & Kilikoglou, 2003).

Supplementary Table 1. Coordinates of the sampling point where each quarry sample of Euganean trachyte was collected.

Supplementary Table 2. Bulk-rock chemical composition of Euganean trachyte determined by XRF for all the samples (quarry number and localization as in Figure 1); major elements are expressed as oxide weight percent, LOI as weight percent, trace elements as ppm and concentrations below detection limit indicated by "b.d.".

Supplementary Table 3. Chemical composition of the main mineral phases in Euganean trachyte determined by LA-ICPMS; major elements are expressed as oxide weight percent, trace elements as ppm and concentrations below detection limit indicated by "b.d." (for data about all the major elements see Table V). Different spot analyses on the same sample (quarry number and localization as in Figure 1) are indicated with progressive numbers and small letters, with outlier samples excluded. Each worksheet contains the results of different phases and average values of the reference materials.

Supplementary Table 4. Complementary binary scatterplots for provenance recognition of Euganean trachyte, based on simple concentrations of major and trace elements of the main mineral phases determined by LA-ICPMS, using the isotopes in Supplementary Table 3. Each worksheet contains the most significant plots for different phases. Quarry symbols as in Table I.

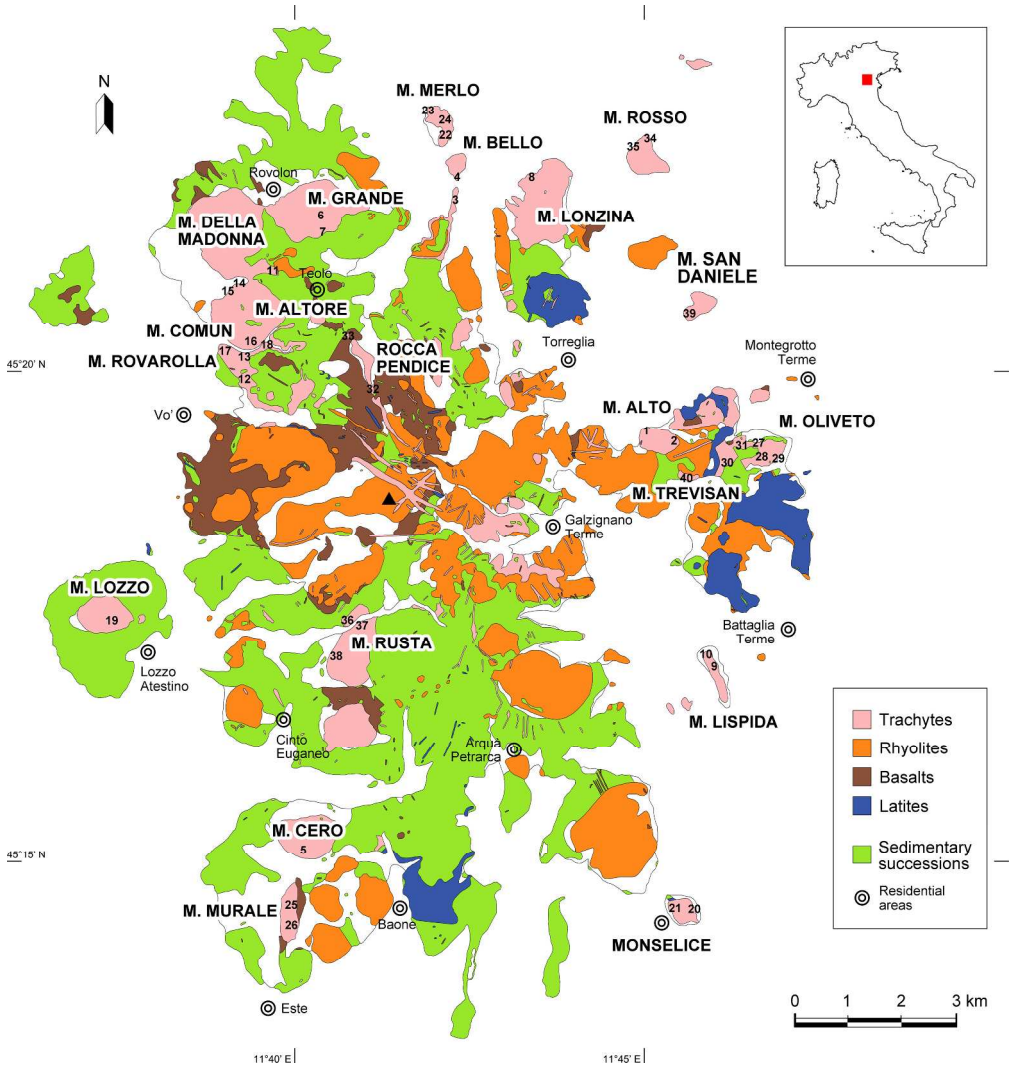

Geological map of the Euganean Hills (modified after Piccoli et al., 1981). The named hills represent the sampled quarry localities, and each of the 40 sampled quarries is marked and localized with a reference progressive number (coordinates of each sampling point in Supplementary Table 1). "M." in the proper name of the hills stands for "Monte" (mount). The peak of the highest hill, M. Venda (601 m a.m.s.l.), is indicated with a black triangle.

Figure 1
130x137mm (600 x 600 DPI)

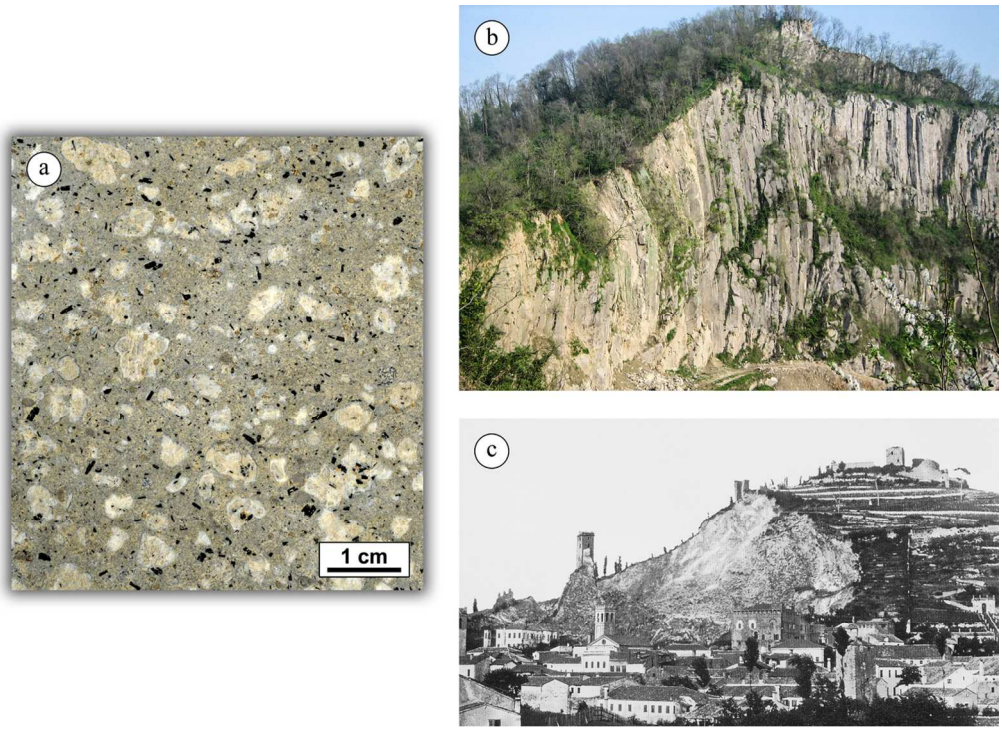

a) Macroscopic appearance of Euganean trachyte (sample from M. Rovarolla); b) quarry face of M. Merlo in 2009, displaying columnar and prismatic jointing (courtesy of Michelangelo Dalla Francesca); c) quarry of Monselice in late 19th-early 20th century (Selmin, 2005): part of the Medieval architectonic complex on the hill has been lost due to excavation activity.
Figure 2
122x87mm (300 x 300 DPI)

Historical use of Euganean trachyte: a) indication of the area of trachyte circulation in the Roman times (shaded) and principal extra-urban roads; b) Roman road with trachyte flagstones in Classe, the ancient port of Ravenna, 4–6th c. CE (Maioli & Stoppioni, 1987); c) funerary stele of Oppi family, Padova, 1st c. CE (courtesy of Musei Civici di Padova, Gabinetto Fotografico); d) Roman rotary querns, Padova (courtesy of Musei Civici di Padova, Gabinetto Fotografico); e) arcade of Palazzo della Ragione, Padova, 13–14th c. CE; f) Basilica of Sant'Antonio of Padova, 13–14th c. CE, with trachyte pillars and buttresses, and on the left the equestrian statue of Gattamelata by Donatello, 15th c. CE, with trachyte base; g) Basilica of San Marco, Venezia, 11th–17th c. CE, in Piazza San Marco, 12th–19th c. CE, paved with trachyte; h) Cologne Cathedral, 13–19th c. CE, with replacing ashlars in Euganean trachyte.

Figure 3
979x1323mm (72 x 72 DPI)

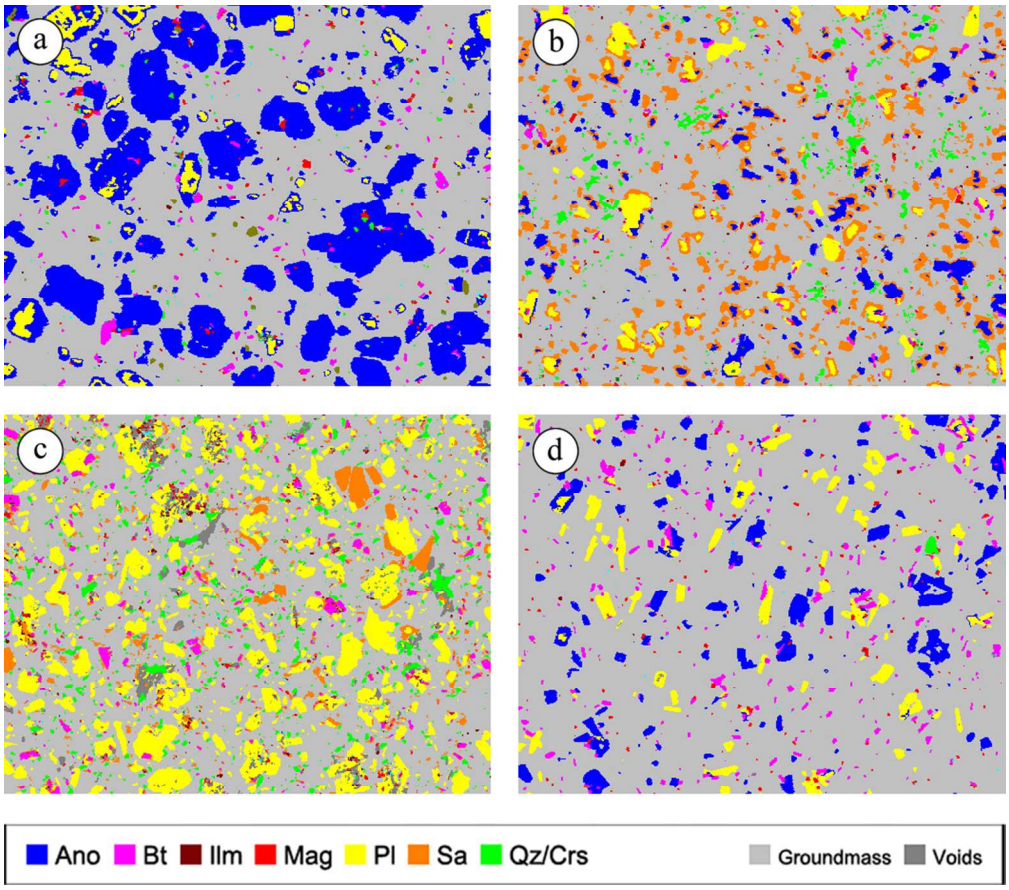

Phase maps of Euganean trachyte processed from X-ray maps acquired by μ-XRF, on a surface of 5.30x4.14 cm of samples from: a) M. Altore, quarry 14, characterized by high concentration of anorthoclase, high P.I. and coarse grain size; b) M. San Daniele, quarry 39, with high amount of sanidine and fine grain size; c) M. Bello, quarry 3, displaying high content of plagioclase and medium-high P.I.; d) M. Cero, quarry 5, with an anorthoclase-plagioclase ratio of ~1:1, low P.I. and fine grain size. Mineral abbreviations as in Table II, colors not in the legend indicate minor phases.
Figure 4
167x146mm (160 x 160 DPI)

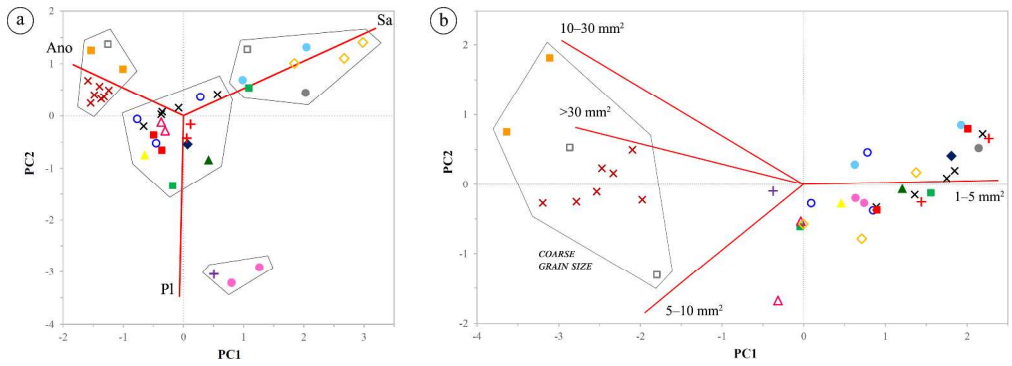

Results of PCA performed on μ-XRF data of trachyte quarries, with score and loading plots built on the following parameters: a) average concentration of feldspars (anorthoclase, plagioclase and sanidine), with PC1 and PC2 covering 49% and 41% of total variance, respectively; b) frequency size classes of feldspars expressed as area, with PC1 and PC2 covering 83% and 10% of total variance, respectively. Quarry symbols as in Table I.

Figure 5

1368x479mm (72 x 72 DPI)

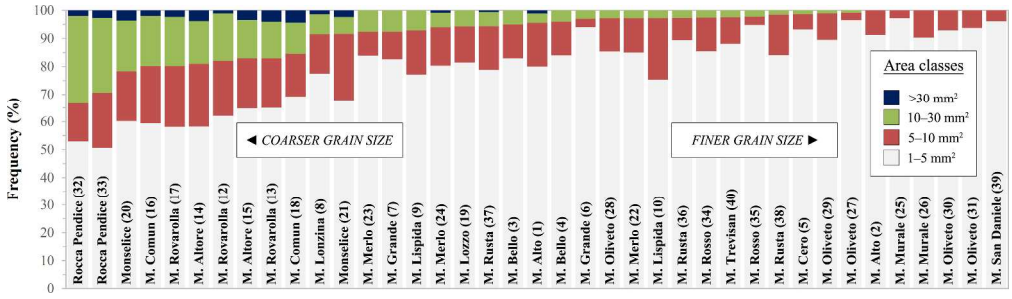

Frequency histogram of size classes of feldspars expressed as area, determined by DIA of μ-XRF maps for each trachyte quarry. Quarries are indicated with locality name and ID number in parentheses.
Figure 6
1579x451mm (72 x 72 DPI)

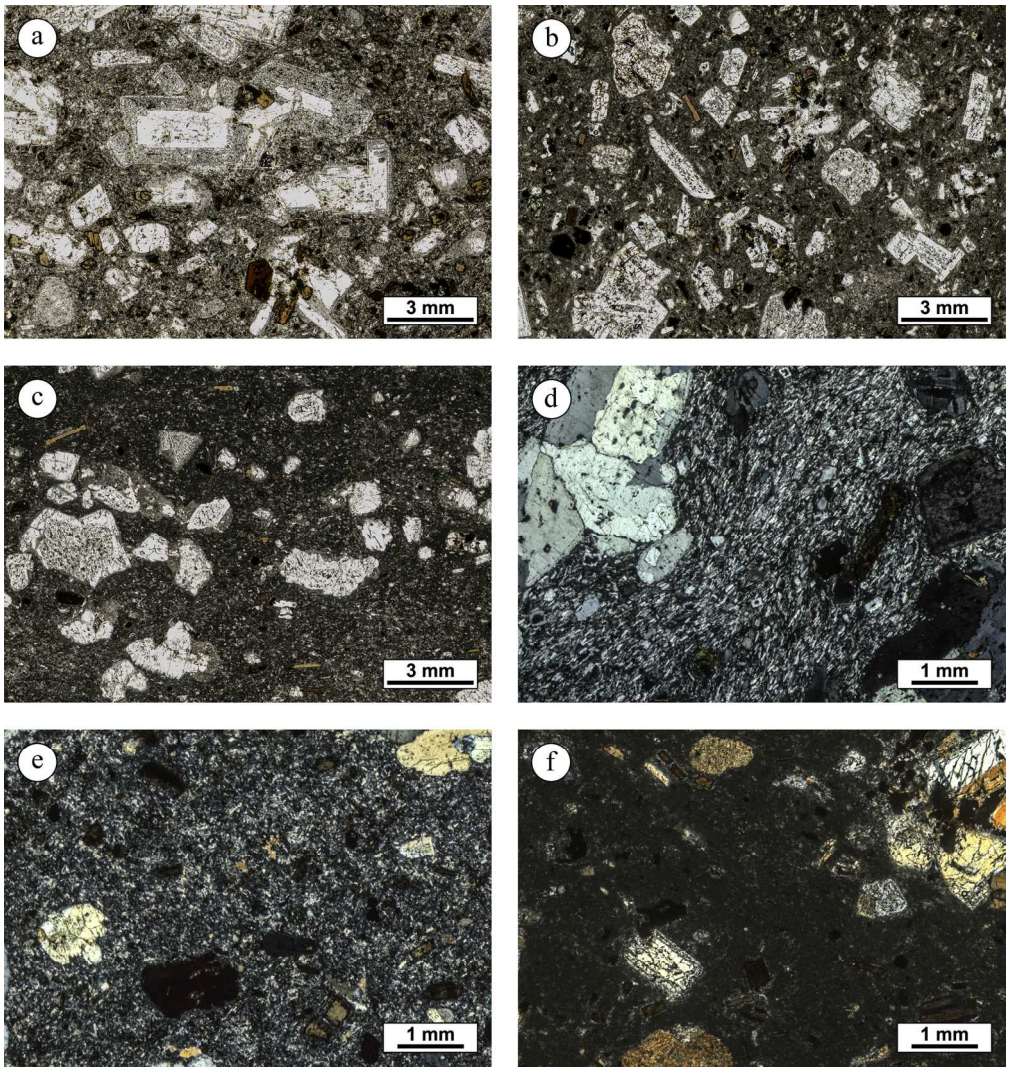

Thin-section photomicrographs of Euganean trachyte, with samples from: a) M. Merlo, quarry 22, showing a seriate grain size distribution (plane-polarized light); b) M. Rosso, quarry 34, displaying a weakly seriate grain size distribution (plane-polarized light); c) M. Oliveto, quarry 31, with a hiatal distribution (plane-polarized light); d) Monselice, quarry 20, having a microcrystalline groundmass with trachytic texture (crossed-polarized light); e) M. Rovarolla, quarry 12, with a microcrystalline felty groundmass (crossed-polarized light); f) M. Oliveto, quarry 30, characterized by a cryptocrystalline groundmass (crossed-polarized light). Anomalous colors are due to the 45 μm thickness of the sections.

Figure 7

180x191mm (300 x 300 DPI)

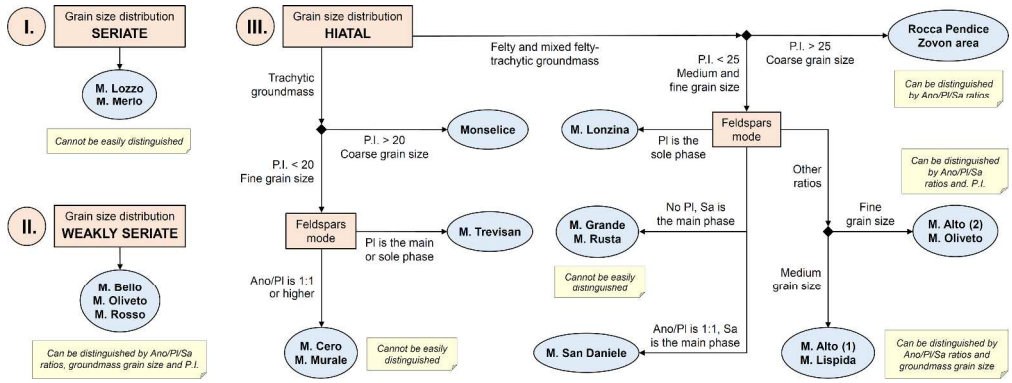

Practical flowchart-like scheme for recognizing quarry locality of provenance of Euganean trachyte, starting from one of the three kinds of grain size distribution. Only few, significant petrographic parameters are considered here, so that it is necessary to refer to the text and tables (Table II, III, IV) for precise attribution, quantitative data and to try discriminating analogous sites. Feldspars abbreviations according to Whitney & Evans (2010).

Figure 8
2271x848mm (72 x 72 DPI)

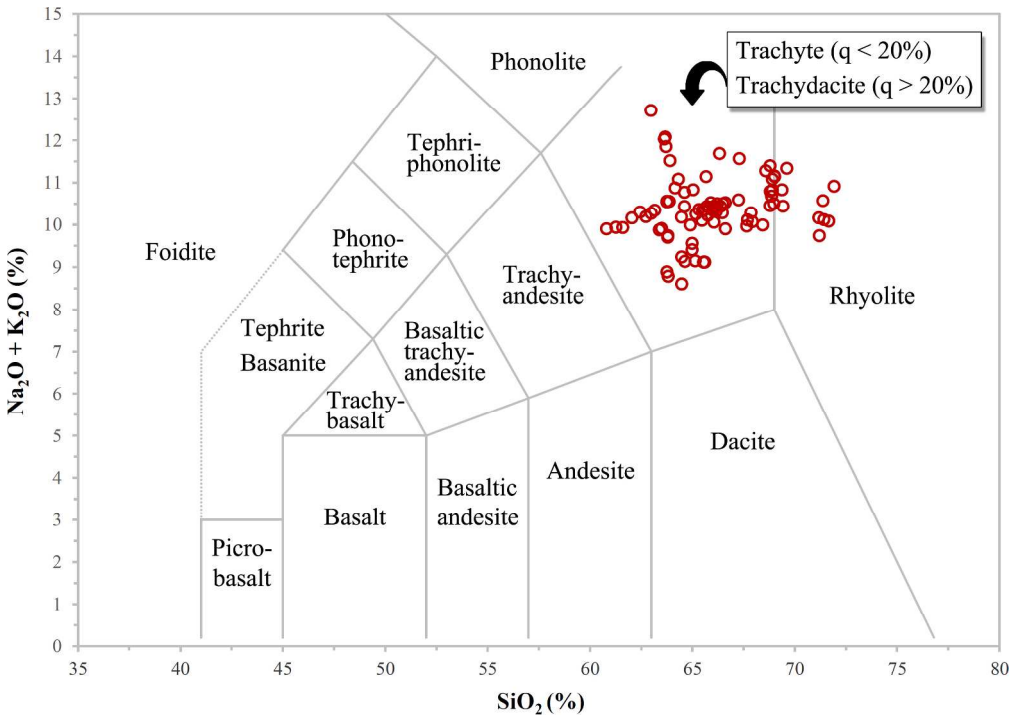

Disposition of the samples of Euganean trachyte in the TAS (total alkali-silica) classification diagram (Le Maitre, 2002), based on bulk-rock chemical composition determined by XRF.
Figure 9
1020x720mm (72 x 72 DPI)

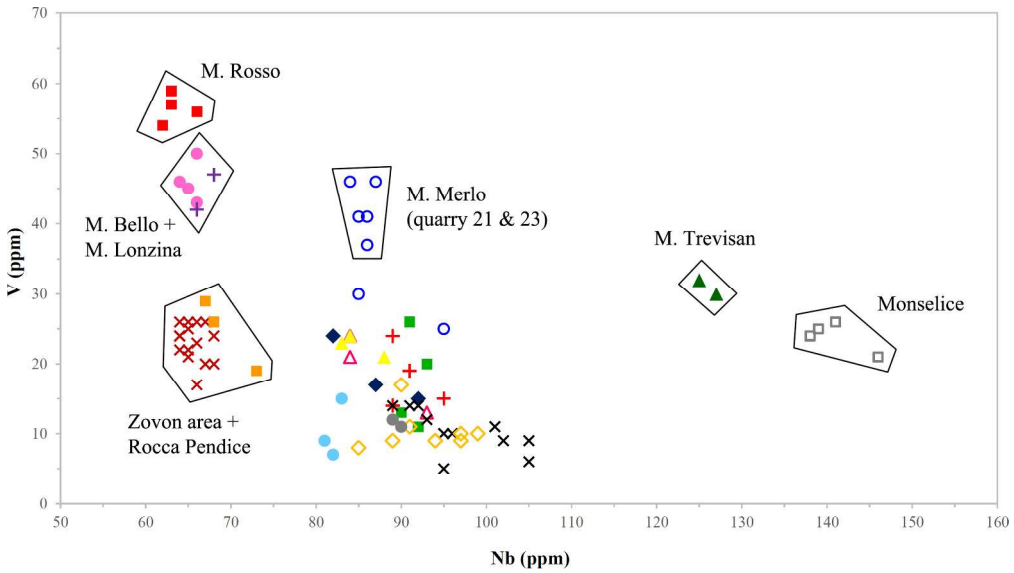

V vs. Nb scatterplot from bulk-rock chemical composition determined by XRF for all the samples of Euganean trachyte. Quarry symbols as in Table I.
Figure 10
1020x571mm (72 x 72 DPI)

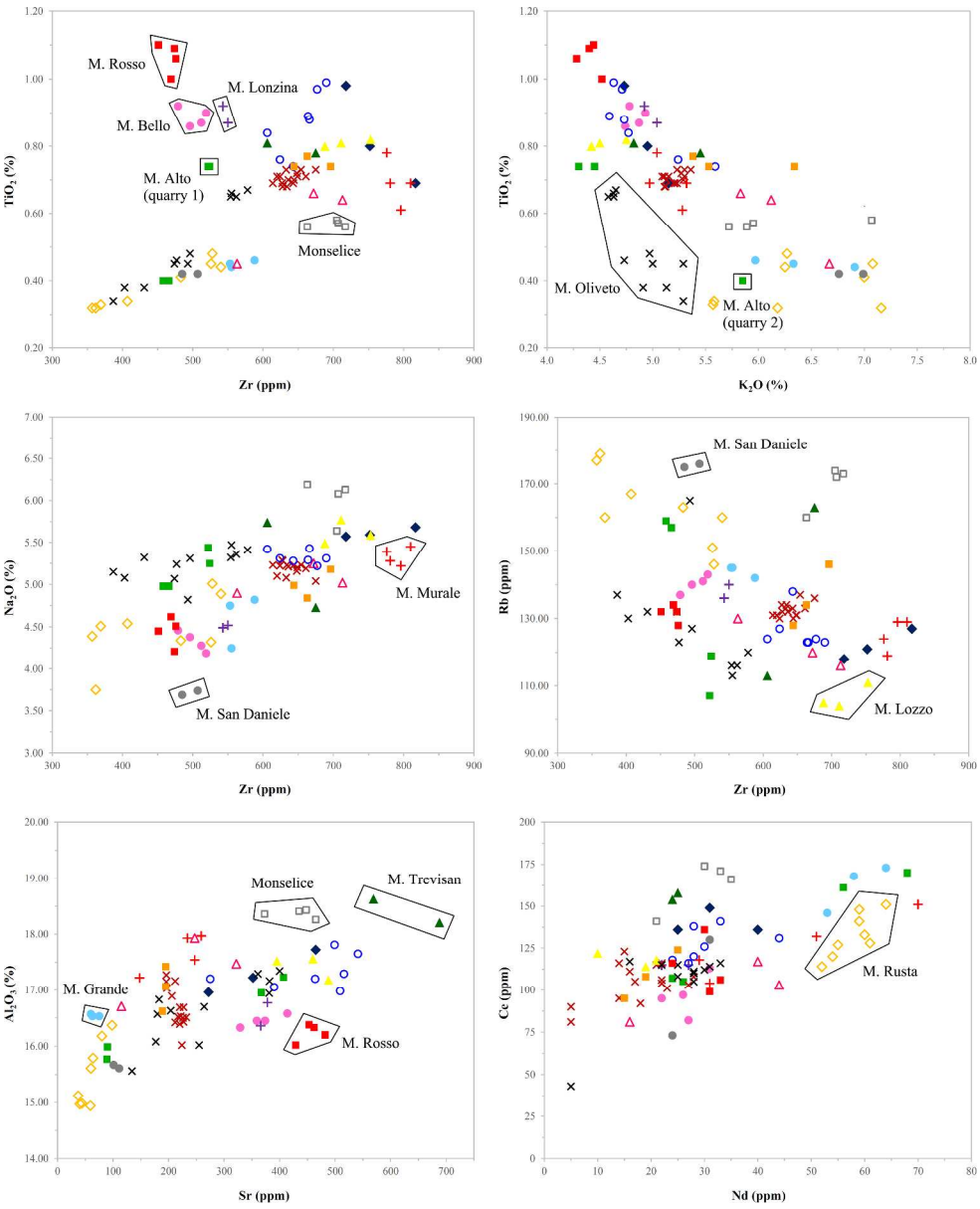

Binary scatterplots from bulk-rock chemical composition determined by XRF for all the samples of Euganean trachyte. Quarry symbols as in Table I.

Figure 11

1954x2398mm (72 x 72 DPI)

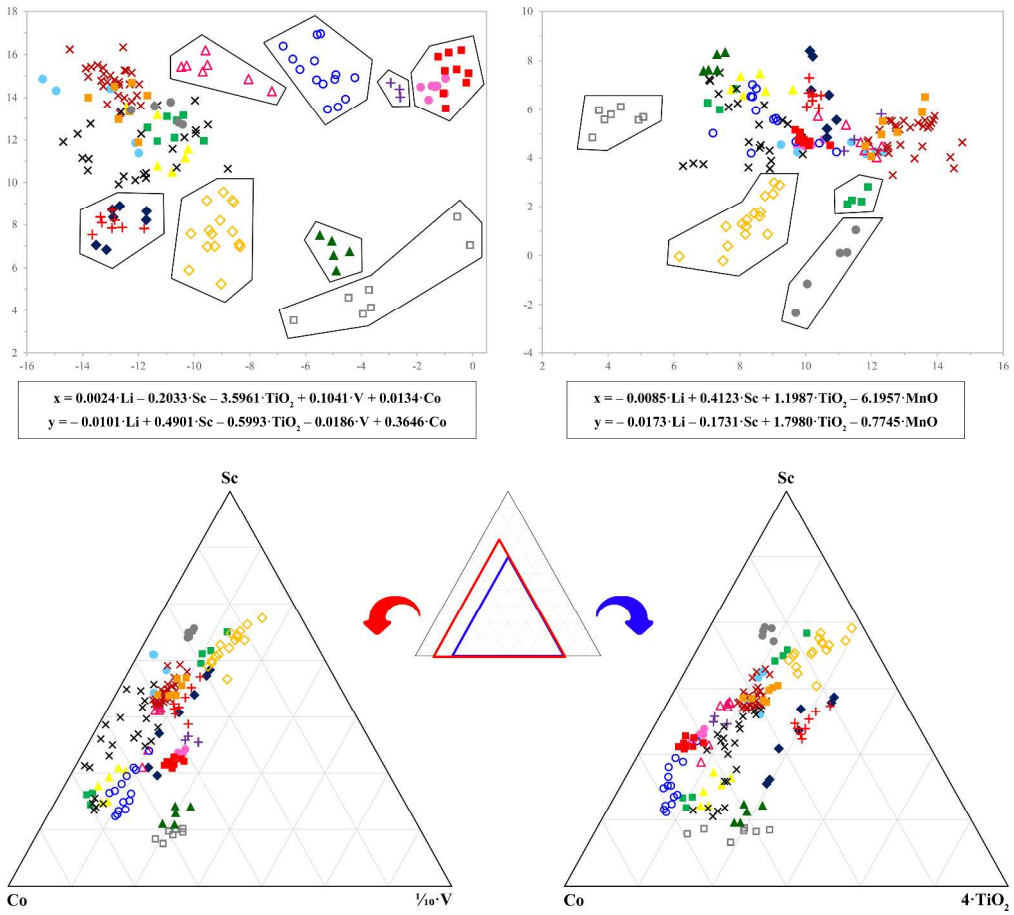

Plots from chemical composition of biotite in Euganean trachyte determined by LA-ICPMS, with major elements expressed as oxide weight percent and trace elements as ppm, using the isotopes in Supplementary Table 3: top) scatterplots after statistical discriminant analysis, with variables calculated from multivariate combinations of element concentrations, indicated under each relevant graph; bottom) ternary plots, scaled up as indicated in the miniature. Quarry symbols as in Table I.
Figure 12
2094x1886mm (72 x 72 DPI)

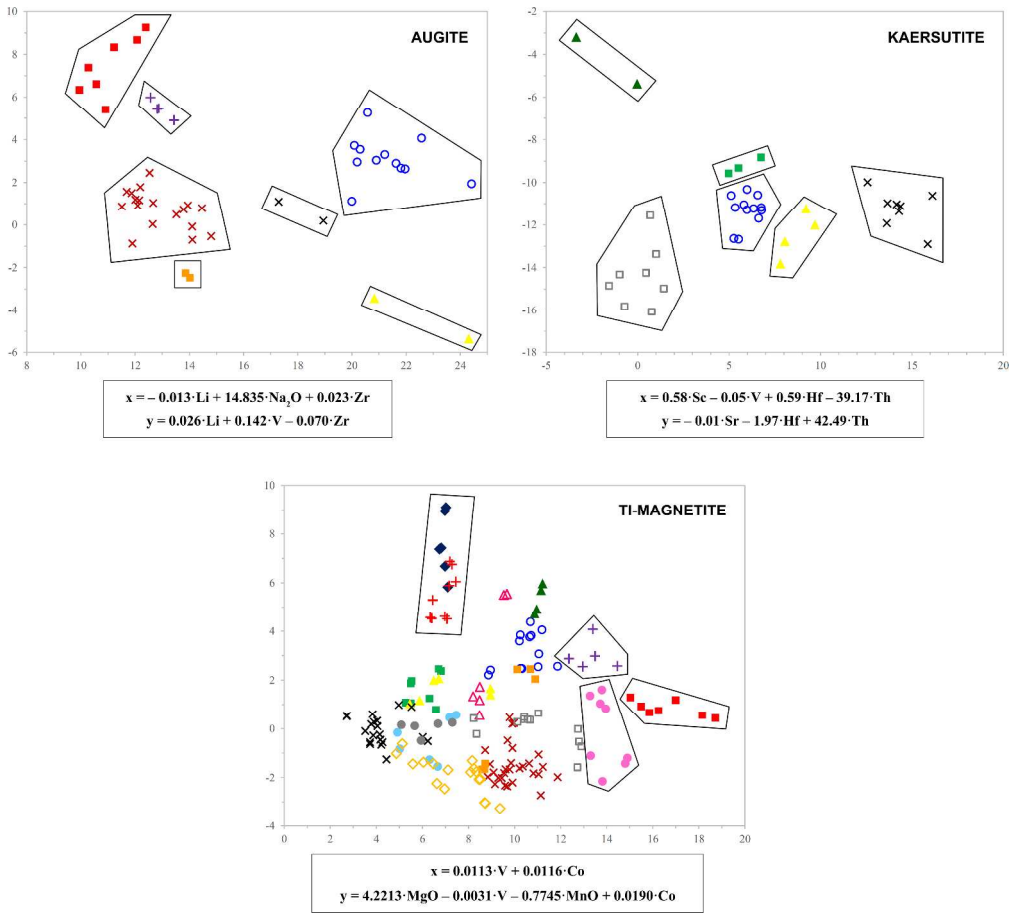

Scatterplots from chemical composition of augite, kaersutite and Ti-magnetite in Euganean trachyte determined by LA-ICPMS, with major elements expressed as oxide weight percent and trace elements as ppm, using the isotopes in Supplementary Table 3; variables are calculated from multivariate combinations of element concentrations, indicated under each relevant graph, after statistical discriminant analysis. Quarry symbols as in Table I.

Figure 13

2095x1894mm (72 x 72 DPI)

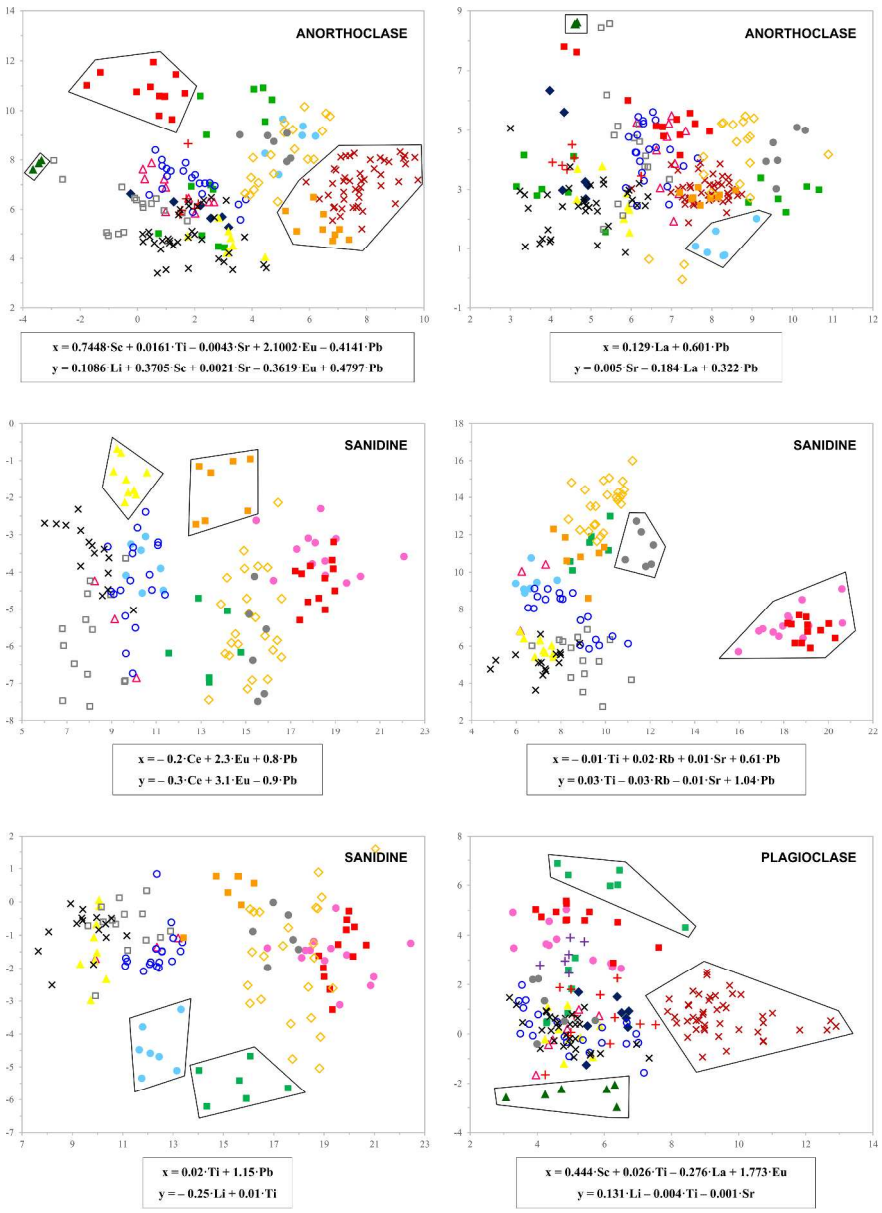

Scatterplots from chemical composition of feldspars in Euganean trachyte determined by LA-ICPMS, with trace elements expressed as ppm, using the isotopes in Supplementary Table 3; variables are calculated from multivariate combinations of element concentrations, indicated under each relevant graph, after statistical discriminant analysis. Quarry symbols as in Table I.

Figure 14

1837x2533mm (72 x 72 DPI)

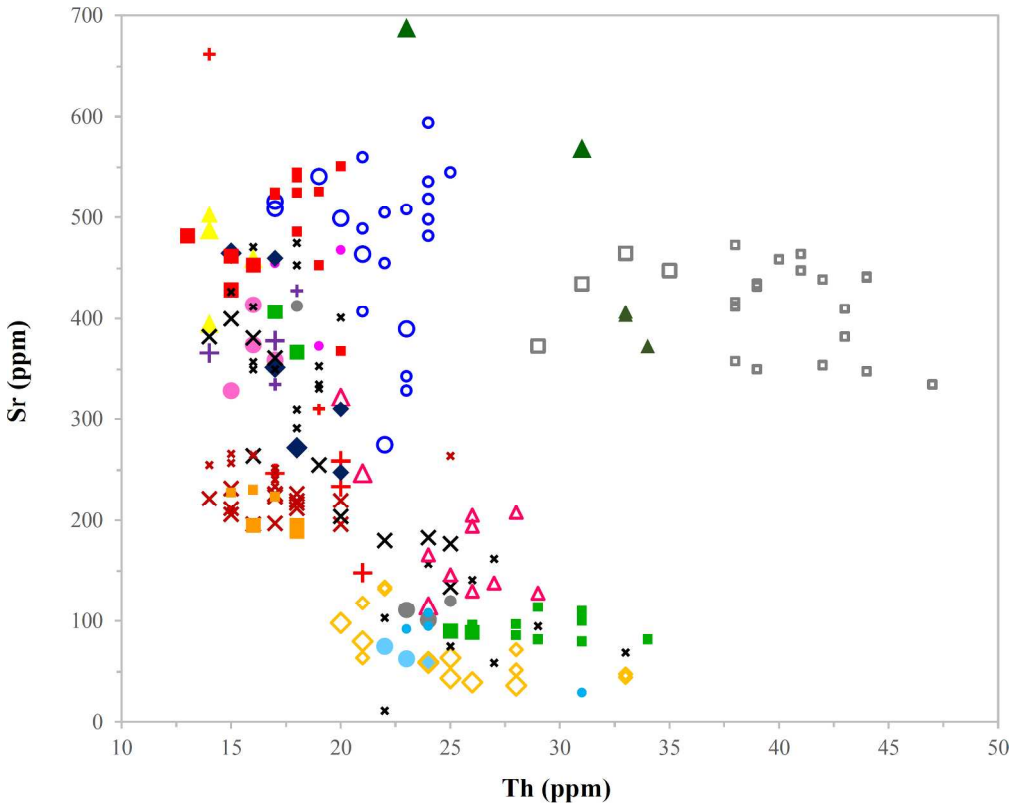

Sr vs. Th scatterplot from bulk-rock chemical composition determined by XRF on Euganean trachyte – the main discriminant diagram by Capedri et al. (2000) – showing the mismatch among the samples from this work (large indicators) and the corresponding ones from the reference database (small indicators). Quarry symbols as in Table I.

Figure 15

1029x818mm (72 x 72 DPI)

Table I. List of the sampled localities and all the 86 samples collected, with relevant quarry specified (identification numbers as in Figure 1; the coordinates of each sampling point are listed in Supplementary Table 1). Each locality is assigned with an identification symbol, used further ahead for plots.

Quarry locality (Hill)	Town	Quarry ID	Sample ID (Quarry)
M. Alto	Torreglia	1; 2	ALT-01, 02 (1); ALT-03, 04 (2)
M. Altore	Zovon di Vo'	14; 15	LTR-06, 07, 08 (14); LTR-09, 10 (15)
M. Bello	Treponti di Teolo	3; 4	BLL-01, 02 (3); BLL-03, 04 (4)
M. Cero	Calaone di Baone	5	CER-01, 02, 03 (5)
M. Comun	Zovon di Vo'	16; 18	LTR-11 (16); LTR-15, 16 (18)
M. della Madonna	Teolo	11	LTR-01 (11)
M. Grande	Rovolon	6; 7	GRN-01 (6); GRN-02, 03 (7)
M. Lispida	Battaglia Terme	9; 10	LSP-01 (9); LSP-02, 03 (10)
M. Lonzina	Luvigliano di Torreglia	8	LNZ-01, 02 (8)
M. Lozzo	Lozzo Atestino	19	LZZ-01, 02, 03 (19)
M. Merlo	Montemerlo di Cervarese S. Croce	22; 23; 24	MRL-01, 02 (22); MRL-03, 04 (23); MRL-05, 06, 07 (24)
M. Murale	Calaone di Baone	25; 26	MUR-01, 02 (25); MUR-03, 04, 05 (26)
M. Oliveto	Montegrotto Terme	27; 28; 29; 30; 31	OLV-01, 02 (27); OLV-03, 04 (28); OLV-05, 06, 07 (29); OLV-08 (30); OLV-09, 10, 11, 12 (31)
M. Rosso	Monterosso di Abano Terme	34; 35	RSS-01, 02 (34); RSS-03, 04 (35)
M. Rovarolla	Zovon di Vo'	12; 13; 17	LTR-02, 03 (12); LTR-04, 05 (13); LTR-12, 13, 14 (17)
M. Rusta	Fontanafredda di Cinto Euganeo	36; 37; 38	RST-01, 02 (36); RST-03, 04, 05 (37); RST-06, 07, 08 (38)
M. San Daniele	Abano Terme	39	SND-01, 02 (39)
M. Trevisan	Montegrotto Terme	40	TRV-01, 02 (40)
Monselice	Monselice	20; 21	MNS-01, 02, 03 (20); MNS-04, 05 (21)
Rocca Pendice	Castelnuovo di Teolo	32; 33	PND-01 (32); PND-02, 03 (33)

- The quarry area of Zovon (M. Altore, M. Comun and M. Rovarolla) is assigned with the same identification symbol, for reasons of high petrographic and chemical homogeneity of the samples and according to Capedri et al. (2000).
- The sample from M. della Madonna turned out to be a petrographic and chemical outlier and has no symbol.

Table II. Modal composition (percentage of mineral phases), groundmass percentage (GM) and porphyritic index (P.I.) determined by μ-XRF mapping and digital image analysis. For each quarry (number and localization as in Figure 1), values are averaged among different samples.

Quarry	Locality	Feldspars				Mafic minerals			Accessory minerals				GM	P.I.
		Ano	Pl	Sa	Σ Fsp	Bt	Aug	Krs	Qz/Crs	Ti-Mag	Ilm	Others		
1	M. Alto	9.44	10.14	-	19.58	2.05	-	0.38	0.38	0.89	0.08	0.44	76.20	23.80
2	M. Alto	3.64	0.36	5.23	9.23	0.37	-	-	1.56	0.27	0.13	0.05	88.39	11.61
3	M. Bello	-	19.33	4.85	24.18	2.07	-	-	4.17	0.47	0.53	0.22	68.35	31.65
4	M. Bello	-	19.75	1.96	21.70	3.09	-	-	2.11	0.12	0.29	0.20	72.49	27.51
5	M. Cero	6.26	4.85	-	11.11	2.57	-	-	0.09	0.67	0.03	0.07	85.45	14.55
6	M. Grande	5.53	-	5.46	10.99	0.50	-	-	3.71	0.63	0.04	0.03	84.09	15.91
7	M. Grande	6.88	-	12.91	19.79	0.65	-	-	1.21	0.28	0.17	0.02	77.88	22.12
8	M. Lonzina	-	17.87	-	17.87	2.24	0.18	-	0.20	1.16	0.30	0.40	77.65	22.35
9	M. Lispida	11.23	4.50	-	15.73	1.49	-	-	0.35	0.41	0.07	0.01	81.94	18.06
10	M. Lispida	12.14	3.75	-	15.88	1.18	-	-	1.70	1.61	0.02	0.04	79.56	20.44
11	M. della Madonna	-	2.89	23.82	26.71	0.91	-	-	4.57	0.38	0.29	0.02	67.12	32.88
12	M. Rovarolla	25.86	2.88	-	28.75	1.60	0.02	-	1.10	0.29	0.07	0.54	67.62	32.38
13	M. Rovarolla	26.99	4.09	-	31.08	1.74	0.53	-	0.19	0.40	0.08	0.95	65.03	34.97
14	M. Altore	28.44	2.81	-	31.25	1.29	0.02	-	0.30	0.62	0.09	0.58	65.85	34.15
15	M. Altore	24.83	3.81	-	28.64	2.18	-	-	0.63	1.02	0.20	0.27	67.07	32.93
16	M. Comun	27.78	5.16	-	32.94	1.57	-	-	1.17	0.22	0.24	0.05	63.82	36.18
17	M. Rovarolla	25.47	4.16	-	29.63	1.58	0.62	-	0.71	0.13	0.34	0.37	66.62	33.38
18	M. Comun	23.84	2.85	-	26.70	1.31	-	-	0.89	0.40	0.16	0.04	70.50	29.50
19	M. Lozzo	16.57	8.51	0.43	25.52	1.59	0.02	0.51	1.80	1.39	0.50	0.21	68.46	31.54
20	Monselice	29.08	-	2.39	31.47	0.25	-	0.15	1.04	1.48	0.37	0.04	65.19	34.81
21	Monselice	12.76	-	9.43	22.19	0.33	-	0.14	0.03	0.74	0.31	0.11	76.15	23.85
22	M. Merlo	14.52	6.88	0.65	22.05	2.15	0.04	0.03	1.29	1.82	0.40	0.23	71.99	28.01
23	M. Merlo	15.93	4.46	6.01	26.41	1.03	0.30	0.32	0.23	0.75	0.31	0.05	70.59	29.41
24	M. Merlo	19.42	5.47	0.96	25.85	1.11	0.69	0.37	0.33	1.10	0.38	0.06	70.09	29.91
25	M. Murale	5.68	2.53	-	8.21	1.43	-	-	0.91	0.62	0.11	0.43	88.30	11.70
26	M. Murale	6.42	4.24	-	10.65	1.46	-	-	0.02	0.42	0.08	0.05	87.31	12.69
27	M. Oliveto	10.00	2.04	0.80	12.83	0.79	-	0.02	0.71	1.09	0.12	0.14	84.31	15.69
28	M. Oliveto	12.52	2.82	0.27	15.60	1.17	-	0.02	1.79	0.50	0.18	0.12	80.62	19.38
29	M. Oliveto	13.52	3.49	0.66	17.68	0.97	-	0.03	4.36	0.31	0.20	0.20	76.24	23.76
30	M. Oliveto	15.99	5.06	-	21.05	1.19	-	-	0.62	0.19	0.25	0.11	76.59	23.41
31	M. Oliveto	7.30	1.21	3.65	12.16	0.62	0.03	0.02	0.67	0.22	0.06	0.08	86.14	13.86
32	Rocca Pendice	21.17	-	0.19	21.36	1.75	1.14	-	0.16	0.57	0.15	0.09	74.77	25.23
33	Rocca Pendice	29.31	-	0.71	30.02	1.31	-	-	0.13	0.86	0.12	0.14	67.43	32.57
34	M. Rosso	14.54	7.94	1.28	23.75	2.17	0.64	-	1.52	1.29	0.31	0.08	70.24	29.76
35	M. Rosso	16.22	6.58	1.18	23.98	2.39	1.23	-	0.86	0.99	0.41	0.07	70.07	29.93
36	M. Rusta	-	-	13.64	13.64	0.71	-	-	2.59	0.36	0.62	0.04	82.05	17.95
37	M. Rusta	2.00	-	16.59	18.59	0.48	-	-	3.79	0.28	0.08	0.01	76.78	23.22
38	M. Rusta	4.14	-	10.31	14.45	0.56	-	-	0.45	0.28	0.10	0.01	84.16	15.84
39	M. San Daniele	4.68	4.04	11.82	20.54	0.86	-	-	2.14	0.42	0.18	0.09	75.78	24.22
40	M. Trevisan	1.56	5.50	-	7.06	0.64	-	0.89	0.65	0.53	0.04	0.38	89.80	10.20

- Abbreviations of minerals according to Whitney & Evans (2010): Ano = anorthoclase; Pl = plagioclase; Sa = sanidine; Bt = biotite; Aug = augite; Krs = kaersutite; Qz = quartz; Crs = cristobalite; Mag = magnetite; Ilm = ilmenite.
- Σ Fsp = percentage sum of all feldspars.
- "Others" include apatite, zircon, titanite, epidote, calcite, dolomite, pyrite and siderite.

Table III. Texture expressed by grain size distribution, observed under the microscope, and size of feldspars (anorthoclase, plagioclase and sanidine considered together) and feldspar glomeroporphyries determined by μ-XRF mapping and digital image analysis. For each quarry (number and localization as in Figure 1), values are averaged among different samples, except for maxima.

Quarry	Locality	Grain size distribution	Feldspars area (mm^2)						Feldspars Feret diameter (mm)				
			Mean	Max	1–5 (%)	5–10 (%)	10–30 (%)	>30 (%)	Mean	Max	≤2 (%)	2–8 (%)	>8 (%)
1	M. Alto	Hiatal	0.78	34.75	80.00	15.56	3.33	1.11	1.19	9.78	83.36	16.09	0.55
2	M. Alto	Hiatal	0.29	9.13	91.30	8.70	0.00	0.00	0.73	6.58	94.11	5.89	0.00
3	M. Bello	± Seriate	0.33	12.17	83.00	12.00	5.00	0.00	0.69	6.29	93.96	6.04	0.00
4	M. Bello	± Seriate	0.57	20.57	84.00	12.00	4.00	0.00	0.96	7.40	89.36	10.64	0.00
5	M. Cero	Hiatal	0.99	10.19	93.24	5.41	1.35	0.00	1.43	5.37	76.92	23.08	0.00
6	M. Grande	Hiatal	0.52	20.99	94.03	2.99	2.99	0.00	0.89	7.56	87.64	12.36	0.00
7	M. Grande	Hiatal	0.56	16.98	82.61	9.78	7.61	0.00	0.97	7.71	89.41	10.59	0.00
8	M. Lonzina	Hiatal	0.98	41.55	77.46	14.08	7.04	1.41	1.15	11.68	85.79	13.96	0.25
9	M. Lispida	Hiatal	0.74	24.19	77.14	15.71	7.14	0.00	1.17	6.98	83.11	16.89	0.00
10	M. Lispida	Hiatal	0.81	13.99	75.34	21.92	2.74	0.00	1.22	6.64	81.78	18.22	0.00
11	M. della Madonna	± Seriate	0.94	23.03	75.44	17.54	7.02	0.00	1.19	8.38	83.00	16.67	0.33
12	M. Rovarolla	Hiatal	1.66	32.51	62.11	20.00	16.84	1.05	1.51	9.77	77.04	22.16	0.79
13	M. Rovarolla	Hiatal	2.21	42.27	65.00	18.00	13.00	4.00	1.73	10.47	71.90	26.14	1.96
14	M. Altore	Hiatal	2.34	70.42	58.23	22.78	15.19	3.80	1.73	15.90	74.74	23.89	1.37
15	M. Altore	Hiatal	1.60	39.06	64.77	18.18	13.64	3.41	1.43	8.84	80.98	17.99	1.03
16	M. Comun	Hiatal	1.63	44.60	59.41	20.79	17.82	1.98	1.47	10.69	78.00	20.63	1.36
17	M. Rovarolla	Hiatal	1.87	42.61	58.14	22.09	17.44	2.33	1.54	11.92	78.67	19.60	1.73
18	M. Comun	Hiatal	1.53	34.35	69.23	15.38	10.99	4.40	1.49	11.04	77.51	20.11	2.38
19	M. Lozzo	Seriate	1.01	29.45	81.45	12.90	5.65	0.00	1.36	10.38	81.33	18.31	0.36
20	Monselice	Hiatal	1.17	40.00	60.24	18.07	18.07	3.61	1.04	10.77	85.56	13.73	0.71
21	Monselice	Hiatal	1.06	41.15	67.86	23.81	5.95	2.38	1.24	10.37	82.67	16.67	0.67
22	M. Merlo	Seriate	0.42	15.37	85.05	12.15	2.80	0.00	0.86	6.15	90.63	9.37	0.00
23	M. Merlo	Seriate	0.62	26.96	83.90	8.47	7.63	0.00	1.01	7.99	87.96	12.04	0.00
24	M. Merlo	Seriate	0.76	34.94	80.34	13.68	5.13	0.85	1.19	9.69	84.72	15.15	0.13
25	M. Murale	Hiatal	0.30	5.60	97.22	2.78	0.00	0.00	0.86	6.23	92.27	7.73	0.00
26	M. Murale	Hiatal	0.47	7.81	90.32	9.68	0.00	0.00	0.88	5.62	89.66	10.34	0.00
27	M. Oliveto	Hiatal	0.40	10.21	96.49	2.73	0.78	0.00	0.88	6.95	91.21	8.79	0.00
28	M. Oliveto	Hiatal	0.40	13.86	85.39	11.80	2.81	0.00	0.84	7.46	92.71	7.29	0.00
29	M. Oliveto	Hiatal; ± Seriate	0.34	13.28	89.53	9.45	1.02	0.00	0.76	8.53	93.23	6.74	0.04
30	M. Oliveto	Hiatal	0.43	9.61	92.92	7.08	0.00	0.00	0.88	7.83	91.10	8.90	0.00
31	M. Oliveto	Hiatal; ± Seriate	0.46	7.22	93.74	6.26	0.00	0.00	0.91	5.51	90.38	9.62	0.00
32	Rocca Pendice	Hiatal	2.23	48.88	52.94	13.73	31.37	1.96	1.67	12.90	77.07	21.95	0.98
33	Rocca Pendice	Hiatal	1.60	44.86	50.67	20.00	26.67	2.67	1.35	12.74	83.04	15.21	1.75
34	M. Rosso	± Seriate	0.52	28.03	85.47	11.97	2.56	0.00	0.93	10.46	89.88	9.92	0.20
35	M. Rosso	± Seriate	0.52	23.55	94.81	2.96	2.22	0.00	1.01	10.83	88.68	11.22	0.10
36	M. Rusta	Hiatal	0.61	15.75	89.47	7.89	2.63	0.00	0.97	7.25	88.33	11.67	0.00
37	M. Rusta	Hiatal	1.23	33.79	78.83	15.55	5.09	0.53	1.51	10.16	76.14	23.41	0.45
38	M. Rusta	Hiatal	0.51	23.93	84.06	14.49	1.45	0.00	0.87	10.04	89.62	10.21	0.16
39	M. San Daniele	Hiatal	0.56	8.89	96.18	3.82	0.00	0.00	1.15	5.15	86.48	13.52	0.00
40	M. Trevisan	Hiatal	0.71	11.88	88.10	9.52	2.38	0.00	1.15	5.45	85.78	14.22	0.00

- Grain size distribution showing intermediate characteristics between hiatal and seriate is marked with "±" (i.e., weakly seriate).
- Area distribution is represented through four classes (with limits at 5, 10, and 30mm^2), Feret diameter distribution through three classes (with limits at 2 and 8 mm) and frequencies within each class are expressed as relative percentage.

Table IV. Groundmass properties: textural arrangement and size of microlites, observed under the microscope, modal composition/glass content expressed in percentage and grain size of SiO_2 phases determined by μ-XRF mapping and digital image analysis. For each quarry (number and localization as in Figure 1), values are averaged among different samples, except for maxima.

Quarry	Locality	Texture	Grain size	Composition							Qz/Crs grain size	
				Afs	Pl	Qz/ Crs	Ti-Mag	Ilm	Glass	Others	Mean area (μm^2)	Mean diameter (μm)
1	M. Alto	Felty	M	72.64	13.27	12.76	0.86	0.07	-	0.39	123.31	15.72
2	M. Alto	Felty	M/C	78.37	-	20.62	0.60	0.23	-	0.18	64.67	10.47
3	M. Bello	Felty	C	74.64	0.38	24.35	0.46	0.14	-	0.03	95.73	15.16
4	M. Bello	Felty	C	69.32	1.24	27.39	0.41	0.28	1.27	0.08	127.39	15.90
5	M. Cero	Trachytic	M	95.01	0.54	3.46	0.77	-	-	0.22	79.97	13.28
6	M. Grande	± Felty	M	81.67	-	16.18	0.43	0.03	1.67	0.01	81.60	12.90
7	M. Grande	± Felty	M	82.70	-	13.84	0.92	0.09	2.42	0.03	102.77	15.62
8	M. Lonzina	Felty	C	78.25	4.81	16.05	0.50	0.33	-	0.07	26.46	7.75
9	M. Lispida	Felty	C	85.59	1.46	7.11	0.99	0.19	4.65	0.01	116.31	11.30
10	M. Lispida	Felty	C/M	86.96	2.38	8.94	0.46	0.12	1.01	0.13	132.00	15.84
11	M. della Madonna	Felty	M	80.27	-	14.43	0.49	0.17	4.35	0.29	49.19	8.15
12	M. Rovarolla	Felty	M	80.71	-	17.96	0.95	0.19	-	0.20	193.55	19.84
13	M. Rovarolla	Felty	M/C	82.22	-	15.13	0.99	0.29	-	1.38	162.17	18.12
14	M. Altore	Felty	M/C	82.09	-	16.13	1.00	0.20	0.29	0.29	179.46	20.05
15	M. Altore	Felty	M/C	80.48	-	17.19	0.80	0.22	1.18	0.13	170.22	19.01
16	M. Comun	Felty	M/C	76.85	-	21.56	0.74	0.24	0.50	0.12	211.26	19.99
17	M. Rovarolla	Felty	M/C	80.31	-	17.17	0.57	0.31	-	1.64	252.77	20.95
18	M. Comun	Felty	M/C	78.30	-	18.42	0.81	0.18	1.81	0.48	184.53	19.92
19	M. Lozzo	Felty	M	78.25	12.38	7.75	0.76	0.36	-	0.51	295.86	19.68
20	Monselice	Trachytic	M	87.47	5.14	4.62	0.66	-	1.21	0.90	176.27	18.35
21	Monselice	Trachytic	M	94.70	2.85	0.03	0.80	-	1.00	0.62	42.53	7.85
22	M. Merlo	Felty	M	74.95	7.36	7.30	0.68	0.34	8.75	0.64	318.03	21.39
23	M. Merlo	Felty	M	72.42	7.08	19.25	0.33	0.57	-	0.34	176.79	18.42
24	M. Merlo	Felty	M	77.03	9.40	12.25	0.61	0.40	-	0.31	425.55	27.02
25	M. Murale	Trachytic	M/C	82.80	11.05	3.39	0.66	0.24	1.73	0.13	30.78	7.39
26	M. Murale	Trachytic	M/C	87.41	8.18	2.81	0.47	-	1.13	0.01	15.61	6.19
27	M. Oliveto	± Felty	C	82.51	-	16.29	0.78	0.25	-	0.17	60.44	12.28
28	M. Oliveto	Felty	C	84.75	-	14.07	0.89	0.17	-	0.12	76.59	11.28
29	M. Oliveto	Felty	C/M	85.81	-	13.14	0.54	0.24	-	0.27	104.72	16.02
30	M. Oliveto	± Felty	C	89.61	-	7.17	0.86	0.23	1.98	0.14	52.48	10.86
31	M. Oliveto	Felty	C/M	85.27	-	14.08	0.36	0.14	-	0.16	35.72	9.13
32	Rocca Pendice	Felty	M/C	88.22	-	10.76	0.78	0.10	-	0.14	106.64	15.47
33	Rocca Pendice	Felty	M/C	81.82	-	14.98	0.56	0.20	2.16	0.27	90.60	12.38
34	M. Rosso	Felty	M	73.85	4.86	20.00	0.64	0.48	-	0.16	127.84	15.93
35	M. Rosso	Felty	M	70.50	4.20	24.15	0.59	0.37	-	0.19	174.72	17.15
36	M. Rusta	Felty	M/C	77.70	-	20.78	0.69	0.17	0.65	-	86.59	13.74
37	M. Rusta	Felty	M/C	84.49	-	14.22	0.62	0.45	0.19	0.03	74.66	13.75
38	M. Rusta	Felty	M/C	83.40	-	15.65	0.33	0.41	0.19	0.02	41.36	9.34
39	M. San Daniele	Felty	M/C	73.37	10.95	12.91	1.23	0.19	1.30	0.05	50.56	10.22
40	M. Trevisan	Trachytic	C/M	72.58	10.83	15.91	0.45	0.04	-	0.20	129.11	14.20

- Texture showing intermediate characteristics between felty and trachytic is marked with "±".
- Grain size is marked with "M" and "C" standing for microcrystalline or cryptocrystalline, respectively.
- Abbreviations of minerals according to Whitney & Evans (2010): Afs = alkali-feldspar; Pl = plagioclase; Qz = quartz; Crs = cristobalite; Mag = magnetite; Ilm = ilmenite.
- Discrimination between alkali-feldspar and plagioclase is uncertain due to their compositions with variable K:Ca ratios.

Table V. Major-element chemical composition of the main mineral phases in Euganean trachyte determined by EPMA and averaged among all the samples with standard deviations (~500 crystals in total); concentrations are expressed as oxide weight percent.

	Anorthoclase	Apatite	Augite	Biotite	Kaersutite	Plagioclase	Sanidine	Ti-magnetite
Na_2O	7.68 ± 0.54	0.30 ± 0.12	0.84 ± 0.26	0.73 ± 0.15	2.76 ± 0.12	7.40 ± 0.73	5.64 ± 0.69	0.03 ± 0.04
MgO	0.01 ± 0.01	0.17 ± 0.11	13.62 ± 1.25	14.21 ± 1.27	12.59 ± 0.70	0.02 ± 0.02	0.01 ± 0.01	0.83 ± 0.77
Al_2O_3	20.79 ± 0.87	0.01 ± 0.02	1.41 ± 0.45	13.84 ± 0.49	12.39 ± 0.61	24.33 ± 1.32	19.13 ± 0.30	1.10 ± 0.66
SiO_2	65.34 ± 1.24	0.29 ± 0.17	51.62 ± 0.68	36.43 ± 0.62	40.39 ± 0.62	60.72 ± 2.09	66.55 ± 0.61	0.75 ± 1.03
P_2O_5	*n/a*	41.77 ± 0.78	*n/a*	*n/a*	*n/a*	*n/a*	*n/a*	*n/a*
Cl_2O	*n/a*	1.12 ± 0.70	*n/a*	*n/a*	*n/a*	*n/a*	*n/a*	*n/a*
K_2O	3.81 ± 1.12	0.02 ± 0.03	0.01 ± 0.01	8.39 ± 0.42	1.05 ± 0.16	1.01 ± 0.29	8.08 ± 0.95	0.01 ± 0.02
CaO	2.25 ± 0.83	53.33 ± 0.62	20.74 ± 0.77	0.03 ± 0.07	10.63 ± 0.29	6.22 ± 1.55	0.54 ± 0.17	0.19 ± 1.12
TiO_2	0.04 ± 0.03	0.01 ± 0.02	0.37 ± 0.14	6.25 ± 0.64	4.83 ± 0.58	0.04 ± 0.03	0.02 ± 0.02	10.83 ± 4.75
Cr_2O_3	0.01 ± 0.02	0.01 ± 0.02	0.01 ± 0.02	0.01 ± 0.02	0.01 ± 0.02	0.01 ± 0.02	0.01 ± 0.01	0.02 ± 0.02
MnO	0.01 ± 0.02	0.26 ± 0.09	1.00 ± 0.33	0.31 ± 0.16	0.26 ± 0.09	0.02 ± 0.02	0.01 ± 0.01	1.03 ± 0.71
Fe_2O_3	0.29 ± 0.08	0.44 ± 0.29	11.04 ± 1.42	16.81 ± 2.27	14.56 ± 1.12	0.38 ± 0.07	0.20 ± 0.05	84.40 ± 6.60